PHILOSOPHICAL TRANSACTIONS A

royalsocietypublishing.org/journal/rsta

Research

Cite this article: Holness MB, Stock MJ, Geist D. 2019 Magma chambers versus mush zones: constraining the architecture of sub-volcanic plumbing systems from microstructural analysis of crystalline enclaves. *Phil. Trans. R. Soc. A* **377**: 20180006.
http://dx.doi.org/10.1098/rsta.2018.0006

Accepted: 16 October 2018

One contribution of 15 to a Theo Murphy meeting issue 'Magma reservoir architecture and dynamics'.

Subject Areas:
petrology, volcanology

Keywords:
magma chamber, enclave, microstructure, crystal mush

Author for correspondence:
Marian B. Holness
e-mail: marian@esc.cam.ac.uk

Magma chambers versus mush zones: constraining the architecture of sub-volcanic plumbing systems from microstructural analysis of crystalline enclaves

Marian B. Holness[1], Michael J. Stock[1] and Dennis Geist[2,3]

[1]Department of Earth Sciences, University of Cambridge, Downing Street, Cambridge CB2 3EQ, UK
[2]US National Science Foundation, 2415 Eisenhower Avenue, Alexandria, VA 22314, USA
[3]Department of Geology, Colgate University, Hamilton, NY 13346, USA

MBH, 0000-0001-9911-8292

There are clear microstructural differences between mafic plutonic rocks that formed in a dynamic liquid-rich environment, in which crystals can be moved and re-arranged by magmatic currents, and those in which crystal nucleation and growth are essentially *in situ* and static. Crystalline enclaves, derived from deep crustal mushy zones and erupted in many volcanic settings, afford a unique opportunity to use the understanding of microstructural development, established from the study of intrusive plutons, to place constraints on the architecture of sub-volcanic systems. Here, we review the relevant microstructural literature, before applying these techniques to interrogate the crystallization environments of enclaves from the Kameni Islands of Santorini and Rábida Volcano in the Galápagos. Crystals in samples of deep-sourced material from both case studies preserve evidence of at least some time spent in a liquid-rich environment. The Kameni enclaves appear to record an early stage of crystallization during

THE ROYAL SOCIETY PUBLISHING

which crystals were free to move, with the bulk of crystallization occurring in a static, mushy environment. By contrast, the Rábida enclaves were sourced from an environment in which hydrodynamic sorting and re-arrangement by magmatic currents were common, consistent with a liquid-rich magma chamber. While presently active volcanoes are thought to be underlain by extensive regions rich in crystal mush, these examples preserve robust evidence for the presence of liquid-rich magma chambers in the geological record.

This article is part of the Theo Murphy meeting issue 'Magma reservoir architecture and dynamics'.

1. Introduction

Over the last few decades, the petrological community has moved away from the idea of sub-volcanic magma being stored in large liquid-rich regions (i.e. magma chambers) towards a model of sub-volcanic plumbing systems that are dominated by hot zones comprising relatively liquid-poor crystal mushes [1–3]. This paradigm shift, largely based on the absence of geophysical evidence for the presence of large bodies of essentially crystal-free liquid underlying currently active volcanoes, raises many fundamental questions. Although there appear to be no large vats of largely liquid magma currently stored in the crust [3], the convincing evidence preserved in the geological record shows that they have existed at other times in Earth history [4]. Furthermore, the geological record preserves evidence of eruption of large volumes of crystal-poor liquid [5]. What governs whether magma occupies big chambers or forms crystal mushy zones? How can large volumes of crystal-poor liquid be assembled if the liquid spends time stored in a crystal-rich mushy zone? Answers to these questions require us to identify such crystal mushy zones in the geological record and to understand how their physical properties (such as rheology and permeability) evolve with time.

In this contribution, we review the evidence preserved in fully solidified intrusions that can be used to distinguish between crystallization in liquid-dominated and solid-dominated systems, showing how outcrop-scale features relate to the associated rock microstructure. We then discuss how to decode the solidification history of small, out-of-context, fragments of disrupted plutonic material entrained in erupted magmas, using their microstructures alone to deduce the crystallization regime active during the lifetime of their deep crustal source. We address the problem via a consideration of microstructural features that can only be formed in systems in which crystals can be re-distributed by magmatic currents (i.e. a system containing a large volume of crystal-poor liquid), and those that indicate *in situ* crystal nucleation and growth (i.e. in a less dynamic system more applicable to a mushy zone). We focus on mafic systems, in which the liquid is relatively low viscosity. Finally, we present two case studies of deep crustal fragments erupted by volcanoes in two distinct tectonic environments—the Galápagos (hot spot setting) and Santorini (arc setting).

2. The petrological signature of a magma chamber

Although there is no evidence to support the existence of such bodies today, it is straightforward to distinguish the endmember magmatic behaviour represented by bodies which formed by the progressive inwards solidification of an essentially crystal-free liquid by examining ancient, fully solidified plutons now exposed at the surface. Inwards solidification is generally manifest in large mafic bodies by a consistent (although often interrupted or repeated) inwards progression from relatively primitive to more evolved compositions [6]. Importantly, such a progression points to efficient fractionation, which is only possible in bodies in which solids can be easily separated from the remaining liquid: it is therefore best developed in liquid-rich bodies of low viscosity magma. The Skaergaard Intrusion of East Greenland epitomizes such behaviour, having crystallized from a large body of crystal-rich magma that was undisturbed by subsequent

replenishment after initial intrusion [4,6,7]. It is important to point out, however, that Skaergaard represents an unusually clear example of crystallization from a liquid-rich magma body: it is not always so straightforward to obtain information on the amount of crystal-free liquid present at each moment during the evolution of the intrusion (i.e. how big the magma chamber was through time).

In smaller mafic intrusions, such as sills, evidence of fractionation of an initially liquid-rich body may be provided by accumulations of dense cargo crystals (pre-existing crystals transported into the reservoir by a carrier melt) on the floor. It has recently been shown that stratigraphic changes in grain size within such accumulations record information about the strength of convection in the magma [8].

On a smaller scale than that of an entire intrusion, fractionation is recorded by compositional zonation towards more evolved compositions on grain margins. Recently, it has been shown that these zoned margins may include a region of constant composition, as a consequence of step-wise thermal buffering along a liquid line of descent in a fractionating system caused by the release of latent heat of crystallization [9] (figure 1*b*). Step-wise changes of the composition of the constant composition zone are present in the stratigraphy of large liquid-dominated bodies such as Skaergaard [9,10]. The sequential arrival of new liquid phases as the remaining bulk magma migrates along the liquid line of descent is also recorded in the stratigraphy of fractionating mafic intrusions by step-wise changes in the augite-plagioclase–plagioclase dihedral angle [11]. Importantly, these methods of detecting the wholesale fractionation of large liquid-dominated bodies require spatial context (i.e. a known position in the intrusion).

The observation of settled blocks with associated disruption of the underlying and surrounding layering [12,13] clearly demonstrates not only the presence of a well-defined floor to a magma chamber, but also that the layering itself must have formed directly at an interface between liquid and mush [12]. Similarly, evidence of scouring and re-deposition of crystals to form modally graded layers [13–15] attests to the actions of magmatic currents on a crystal mush forming on the floor of a crystal-poor magma chamber.

Fabrics defined by a shape-preferred orientation, defining either a lineation or foliation, form in a liquid-rich environment either during settling or by re-arrangement at the interface between the mush and the overlying magma [16]. A fabric created during crystal accumulation in a liquid-rich environment is indicated by the juxtaposition of undeformed euhedral grains (i.e. bounded by growth faces) cemented by anhedral interstitial material (figure 1*a*) [14]. Fabrics and microstructures indicative of grain accumulation on the floor of a liquid-rich chamber are typical of modally graded layers in plutons ranging from gabbros [12–14] to granodiorite [16]. Fabrics may also form in a crystal-rich environment, by shear caused by wholesale pre-consolidation slumping [17–21] or during grain-supported flow during pluton-scale events [22]: these are typically not associated with modal layering.

3. How can we study crystal mushy zones?

The abundant and convincing evidence described above supports the existence of melt-rich magma chambers in the plutonic record and has shaped our thinking for decades about what is happening in the magmatic plumbing systems of currently active volcanoes. The new ideas suggesting that magma chambers are not present under currently active volcanoes [3] mean that we should not rely on models based on this type of magma storage zone but need instead to find another way of interrogating the deep crust in volcanic regions. One direct source of information is provided by entrained fragments of incompletely solidified cognate mush, derived from depth in the magma source region and found in erupted magmas. These have a range of names in the literature, including cognate xenoliths or nodules: here, we will refer to them as glassy crystalline enclaves or simply enclaves. These entrained fragments of deep mush are relatively common in the eruptive products of currently active or recent volcanoes [23–31] and can inform us about the magmatic plumbing system in the present day. Fully solidified (i.e. non-glassy) non-erupted

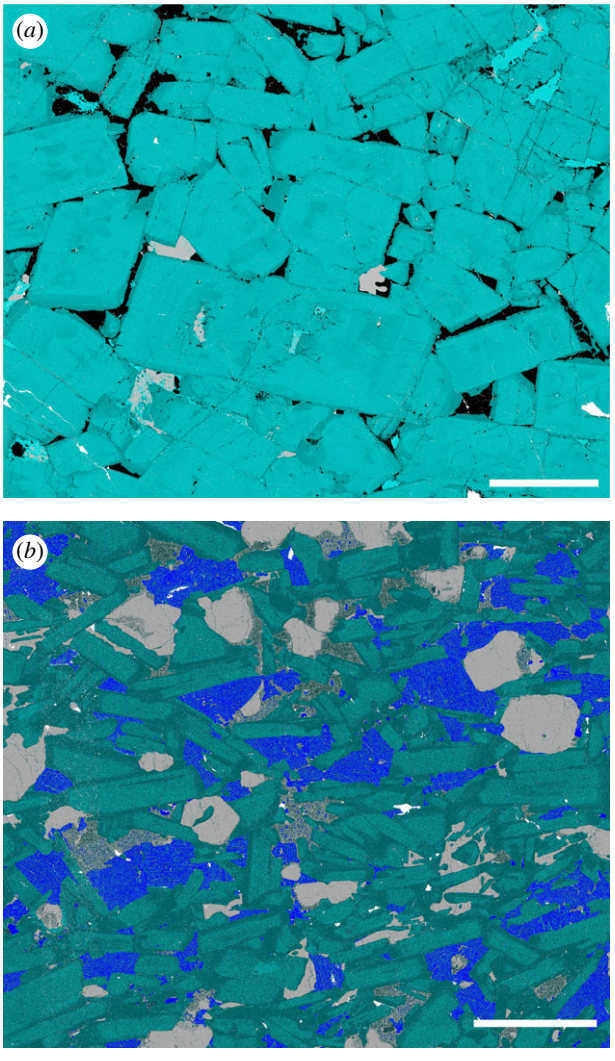

Figure 1. QEMSCAN maps of Ca distribution in cumulates from the Layered Series of the Skaergaard Intrusion, East Greenland. (*a*) The leucocratic portion of a modal layer from Trough G in Upper Zone. Plagioclase is teal (with darker colours showing more sodic compositions), interstitial phases are quartz (black) and clinopyroxene (grey). Note the euhedral shape of the plagioclase, with most grain boundaries formed by the juxtaposition of these planar growth faces. Although some boundaries show evidence of indentation, the smoothness of these boundaries and the localized presence of late-stage albite on them, together with the absence of a preferred orientation of the late-stage albitic overgrowths on the plagioclase, demonstrates that these indentations are not a consequence of dissolution–reprecipitation in response to an applied stress but are most likely a consequence of irregular, late-stage growth of grains accumulated on the magma chamber floor. The scale bar is 1 mm long. (*b*) A troctolitic cumulate from Lower Zone. Plagioclase is dark teal, with dark relatively albitic rims. Olivine is grey and augite is bright blue. Low-Ca pyroxene (inverted pigeonite) is a mottled grey. The cores of the plagioclase grains formed close to the magma–mush interface, while the constant composition's relatively sodic rims formed within the mush. The scale bar is 2 mm long.

examples of entrained deep-sourced plutonic material may also be exposed by erosion in older settings (e.g. xenoliths in the Skaergaard Campsite Dyke [10,32]).

In contrast to the study of fully solidified plutons, in which spatial information is available at all scales, there is no spatial context for entrained glassy crystalline enclaves: we need therefore to emulate the scientists who decoded rocks brought back from the Moon during the lunar programme and rely on information encoded in the enclaves themselves. In the past,

geochemistry was used as the primary tool to determine the genetic relationships between enclave and host, and to place the enclaves in a wider igneous setting [31]. Geochemical techniques for constraining the pressure and temperature of crystallization are well known [33] and will not be addressed here. Instead, we will focus on microstructure, which is a relative newcomer to the field. Previous work on this subject has investigated melt distribution in glassy crystalline enclaves [34], but here we also include a consideration of microstructural proxies for cooling rate and fluid dynamical regime during crystallization. This review highlights what we currently know about the environment of enclave formation, using case studies to illustrate our current position (which is dominated by work on mafic rocks) and points to where more work is needed to fully decode the enclaves' record of magmatic processes in a robust and quantitative way across the range of magma compositions.

4. Are entrained fragments representative of the deep plumbing system?

Entrainment and eruption of a representative sample of the deep regions of a magmatic plumbing system is not straightforward. Perhaps the most fundamental issue concerns the Stokes settling velocity: large, dense, enclaves are less likely to be erupted compared to smaller, buoyant, enclaves, creating a sample population biased towards the more silicic material. Such a bias may be evident in the population of xenoliths entrained in the Campsite Dyke in the Skaergaard intrusion [10,32], in which the largest enclaves are plagioclase-rich, while the more mafic examples tend to be the smallest (M.B. Holness, unpublished data). However, in relatively volatile-rich systems, enclave bulk density may be reduced by significant gas exsolution which, if it is not sufficient to disintegrate the enclave (see discussion below), may promote ascent [35].

Entrainment involves the mechanical process of fracturing and dislodging material from its source and this is poorly understood. Of particular relevance is the possibility that the ease of entrainment varies with the geometry, size and orientation of the interface between the ascending magma and the material to be entrained. For example, it is possible that entrainment is easier at vertical surfaces such as conduit walls compared with the floor of a magma chamber. Although the predominantly laminar flow in narrow dyke-like conduits [36] is perhaps ineffective in causing entrainment of side wall material, entrainment might be more efficient if subsequent injections of magma resulted in re-opening (by brittle failure) of an older conduit.

Various lines of evidence have been used to infer that enclaves were derived from the chilled side wall of their source magma body, such as differences in the primocryst assemblages between the enclaves and host magma [25]; a higher concentration of enclaves in the earlier parts of the eruption [25]; the presence of intrusive contacts between mush and country rock within enclaves [28]; microstructures characterized by loose, high-porosity, frameworks that can be attributed to inwards growth in vertical solidification fronts [25,28]; and a fine grain size and low glass content relative to that in the enclave population as a whole [29]. Although the presence of contacts within the enclave certainly provides incontrovertible evidence that it did indeed derive from the margin of the source body, the other criteria were devised in the context of a paradigm in which eruptions are fed by magma chambers in which solidification occurred on their (vertical) walls, while crystals accumulated on a (horizontal) floor. They should be re-visited in the light of our new conception of mushy sub-volcanic magma storage regions.

Survival of entrained material during ascent necessitates minimal disaggregation: the survival of crystal-rich fragments therefore depends on their ability to withstand the shearing forces imposed by the magma and the tensile forces due to vesicle expansion. The latter is not only due to the reduced solubility of H_2O and CO_2 with decreasing pressure, but also due to the expansion of gas during ascent. These effects become highly significant at pressures lower than a few hundred MPa [37], even for relatively H_2O-poor liquids. Since rocks, especially those that are incompletely solidified, have low tensile strengths, enclaves will disintegrate during ascent unless this expansion can be accommodated by the loss of either gas or interstitial melt (e.g. gas filter-pressing [38]). The first relies on the formation of interconnected bubble chains, which occurs above approximately 30 vol.% gas [39]. The second relies on the enclave containing

sufficient interstitial melt to accommodate vesicle expansion by melt expulsion—this results in the development of glass-rich rinds on enclaves [40].

This bias in enclave survival is the most likely reason behind the observation that enclaves generally have greater than 60 vol.% crystals, reflecting the minimum volume fraction of crystals at which a framework of randomly oriented prismatic grains (the dominant texture of high-porosity nodules) retains its integrity during ascent. The bulk volumetric proportion of vesicles in enclaves is generally less than 30 vol.% [29,35,41], either due to the strength reduction of the high-porosity enclaves at higher vesicle contents or because this represents the percolation threshold above which vesicles form an interconnected network permitting the escape of the excess gas volume [39].

The population of erupted enclaves may therefore not be representative of the crystal mush at depth. The population will be biased towards regions of the mush which are most easily broken to form discrete fragments, with a further bias introduced during ascent: the enclaves that easily disintegrate contribute to the phenocryst load (as xenocrysts or antecrysts) rather than erupting as discrete entities.

5. Microstructural proxies for cooling and crystallization rates

To determine the source of an enclave, we need to differentiate between enclaves derived from the conduit along which the magma travelled and those entrained from the larger magma body feeding the conduit. Conduits are likely to be relatively rapidly cooled due to their limited lateral extent. Consequently, if the enclaves preserve evidence of slow cooling and crystallization, they are more likely to come from a larger body. Enclaves are typically less than 1–10 cm in scale, with rare larger examples provided by the Skaergaard Campsite Dyke xenoliths. Indicators of cooling and crystallization rates therefore need to be applicable to such small samples. A commonly used geochemical method to constrain the cooling rate of such small samples depends on the analysis of diffusional modification of step-changes in mineral composition [42]: here, we describe alternative methods based on microstructure.

(a) Retention of high-temperature crystallographic structures

Some minerals, such as low-Ca pyroxene and quartz, undergo reconstructive phase transitions during cooling. If cooling happens too quickly for the phase transition, then the high-temperature form is retained at low temperatures. An example of this is observed in cognate gabbroic xenoliths in the Skaergaard Campsite Dyke. This dyke intruded the upper levels of the Skaergaard cumulate stratigraphy, while the intrusion was still hot, entraining material from deeper levels in the intrusion. Although all pigeonite in the cumulate stratigraphy of the Skaergaard intrusion is fully inverted to orthopyroxene, those pigeonite primocrysts in the gabbroic xenoliths entrained in the dyke are only partially inverted [10], demonstrating that they were relatively rapidly cooled, preventing completion of the reconstructive phase transition from the monoclinic to the orthorhombic structure.

(b) Plagioclase grain shape

Plagioclase is an especially informative mineral for reconstructing magmatic processes: it is the most abundant mineral in the Earth's crust; the slow diffusion rates of the major components preserve compositional zoning, and record episodes of growth and dissolution; its generally tabular shape results in shape-preferred orientations that provide information about magmatic flow [14,15]; and the shape itself can be used to decode crystallization timescales.

The shape of plagioclase grains growing from a liquid is dependent on the extent of departure from equilibrium, which is in turn dependent on the extent of undercooling [43]. At large undercoolings, diffusion-limited growth results in swallowtail and spherulitic forms, whereas facetted euhedral grains form at low undercoolings when growth is interface-controlled. The

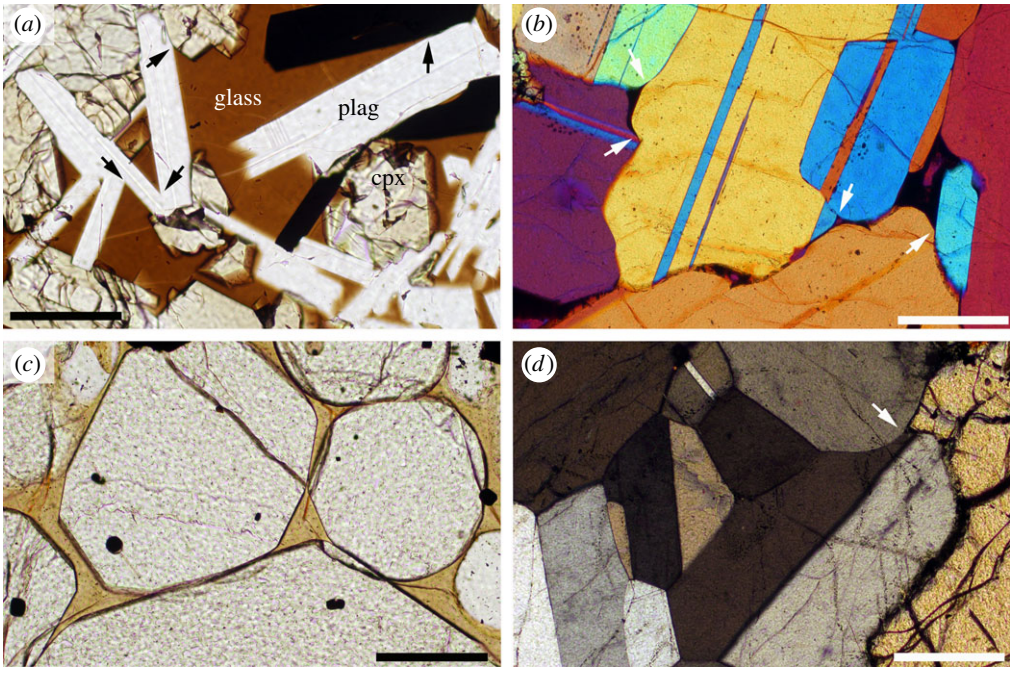

Figure 2. (*a*) Glass-rich portion of the upper crust of the Kilauea Iki lava lake, quenched during drilling. Plagioclase (labelled plag), augite (labelled cpx) and ilmenite (opaque) form a framework with interstitial brown glass (labelled glass). The junctions between adjacent grains are formed by the meeting of planar growth faces (examples are arrowed) with no evidence for minimization of interfacial energies. Plane polarized light. Scale bar is 1 mm long. (*b*) Plagioclase-rich glassy enclave from Brandur, Iceland, photographed with sensitive tint plate under crossed polars. The glass-filled pores have rounded cuspate margins, with low, equilibrium values of the melt–plagioclase–plagioclase dihedral angle established at pore corners (examples are arrowed). Scale bar is 0.5 mm long. (*c*) Olivine-rich glassy enclave from Mauna Loa, Hawaii. The rounded olivine grains display dihedral angles close to textural equilibrium at pore corners. Plane polarized light. Scale bar is 0.5 mm long. (*d*) Troctolitic cumulate from the Eastern Layered Intrusion of the Rum Igneous Complex, Inner Hebrides. Three-grain junctions involving only plagioclase are close to textural equilibrium, with a well-developed granular microstructure in plagioclase-only regions. Note the absence of any evidence of planar plagioclase growth faces, in contrast to figure 1*a*. The olivine grain on the right has a low dihedral angle where it forms a three-grain junction with two plagioclase grains (arrowed), demonstrating an absence of textural equilibration of this poly-phase junction. Crossed polars. Scale bar is 0.5 mm long.

shape of euhedral plagioclase grown at low undercoolings, quantified by the average apparent aspect ratio (AR) as observed in thin section, is a systematic function of crystallization time [44]. The average apparent AR shows a well-defined negative correlation with the time taken to crystallize. Hence, we can use AR to determine the *minimum* size of the body from which any enclaves were derived.

(c) Grain junction geometry

(i) Melt–solid–solid junctions

The shapes of grains, and the geometry of intervening melt-filled pores, in solidifying materials are generally determined by the kinetics of crystal growth. At the crystallization rates experienced in plutonic environments, growth is interface-controlled, and most minerals of geological relevance grow with planar faces: the geometry of melt-filled pores is therefore governed by the impingement of these planar-sided grains (figure 2*a*). Such a microstructure has a high total interfacial free energy in comparison to texturally equilibrated microstructures which

are characterized by smooth curvature of melt–solid interfaces and the establishment of the equilibrium melt–solid–solid dihedral angle at pore corners (figure 2*b*,*c*). The driving force for textural equilibration is the reduction of interfacial energies, which is generally much smaller than the driving force for chemical equilibration (i.e. crystallization). Therefore, solidifying systems only approach textural equilibrium if the rate of crystallization is slow or reduced to zero [45].

Textural equilibration is achieved first at pore corners, by rotation of large areas of the melt–solid interfaces to create the equilibrium dihedral angle: the corresponding curvature of the interfaces then propagates outwards from the two-grain junctions [46]. The rate at which this equilibration process occurs is not well known: although experiments suggest that equilibrium can be achieved in olivine-basalt aggregates with a grain size of order 0.1 mm within a week [45], grain growth in these experimental charges obscures the timescales of the establishment of constant mean curvature at the interfaces. Establishing the rates at which textural equilibrium is approached in the super-solidus should be a focus for future work.

(ii) Three-grain junctions

The median dihedral angle at three-grain junctions involving only a single phase is, by geometrical necessity, 120°. The extent of textural equilibration cannot, therefore, be ascertained simply from the median of the dihedral angle population, but must be assessed from a consideration of the extent to which the grain boundaries have constant mean curvature, and from the standard deviation around the median dihedral angle: for isotropic materials this will be zero, increasing commensurately with increasing crystallographic anisotropy of the mineral [47]. In shallow crustal rocks, single-phase three-grain junctions are commonly close to textural equilibrium, whereas the dihedral angles at junctions involving two phases are generally far from equilibrium (figure 2*d*). This difference in the amount of sub-solidus modification of primary igneous microstructures is because equilibration of multi-phase junctions involves significant mass transport along grain boundaries whereas the overprinting of the primary crystallization geometry at single-phase junctions requires only the migration of grain boundaries [46].

The microstructural usefulness of plagioclase is further exemplified by the systematic variation in the median value of the disequilibrium augite-plagioclase–plagioclase dihedral angle with the cooling rate in mafic intrusions [48]. Augite-plagioclase–plagioclase dihedral angles vary because of the way crystallization rate affects the rate at which the different plagioclase faces grow [49] (which, as we have seen, also controls the final shape of plagioclase grains [44]). Because the anisotropy of plagioclase growth is the primary control on disequilibrium dihedral angles, we would expect any three-grain junction involving two grains of plagioclase and a grain of a second phase to show the same systematic variations with crystallization timescales, as long as the morphology of the second phase did not also have a strong cooling rate control [49].

6. Melt distribution in the crystal mush

The distribution of glass in incompletely crystallized (predominantly mafic) enclaves has been investigated by Holness *et al*. [34]. They found that melt is very commonly present as thin films on grain boundaries (figure 3*a*). The films do not have parallel sides and locally contain small mineral grains, demonstrating that they are primary and were not created by decompaction during ascent. Holness *et al*. also identified features that they termed ‘impingement lenses’: these are small cuspate pockets of glass on irregular grain boundaries, interpreted to result from the growth of the two bounding grains into the remaining intervening pore space (figure 3*b*–*d*) [34]. Importantly, Holness *et al*. demonstrated that the shape of late-crystallizing interstitial phases in fully solidified gabbros is consistent with these late-crystallizing phases infilling and pseudomorphing the last remaining pockets of melt, arguing that the glass distribution in the super-solidus enclaves is indeed indicative of that in almost fully solidified gabbros [34].

Enclaves that were fully crystallized before entrainment can also sometimes betray where the last melt was, if the host magma that brought them to the surface was sufficiently hot to trigger

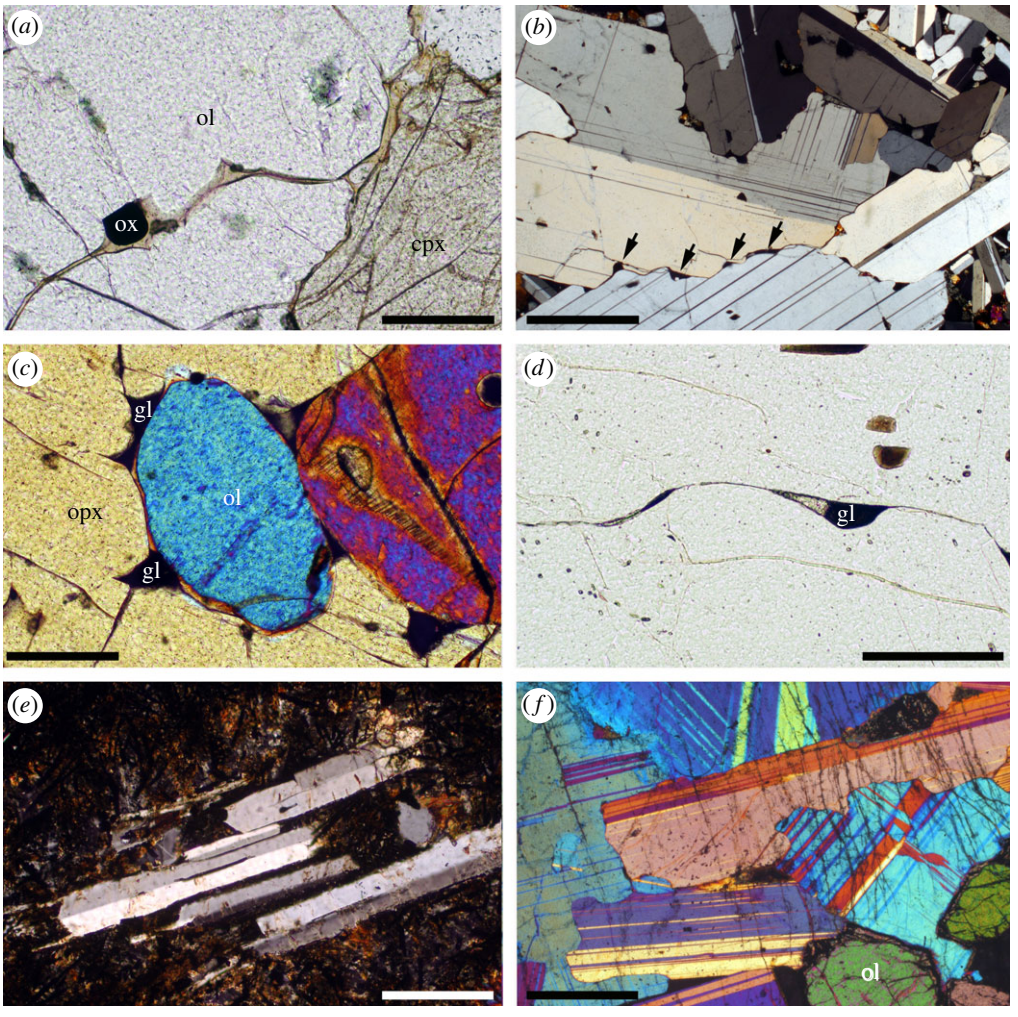

Figure 3. (*a*) Glassy crystalline enclave from Mauna Loa, Hawaii, with an irregular glass film separating grains of olivine (ol) and augite (cpx). Note the small grain of spinel (labelled ox) sitting in the melt film, demonstrating its primary origin during solidification. Plane polarized light. Scale bar is 0.5 mm long. (*b*) Plagioclase-rich glassy enclave from Brandur, Iceland, showing lenses of glass (examples are arrowed) on irregular grain boundaries. Crossed polars. Scale bar is 1 mm long. (*c*) Glassy crystalline enclave from Mauna Loa, Hawaii, with irregular glass pockets (some of which are labelled gl) on boundaries between olivine and orthopyroxene (labelled opx). Note the low dihedral angles at pore corners, denoting approach to super-solidus textural equilibrium. Crossed polars. Scale bar is 0.5 mm long. (*d*) Plagioclase-rich enclave from Brandur, Iceland, showing a small pocket of glass on a plagioclase–plagioclase grain boundary, now partially infilled by clinopyroxene. Plane polarized light. Scale bar is 0.5 mm long. (*e*) The chilled margin of the Bracken Bay-Straiton Dyke, SW Scotland, showing a cluster of plagioclase phenocrysts set in a fine-grained groundmass. Note the alignment of the plagioclase and that they are joined along large areas of planar grain boundary parallel to the growth faces. Crossed polars. Scale bar is 0.5 mm long. (*f*) Gabbro from the Marginal Border Series of the Skaergaard Intrusion, East Greenland, showing highly irregular grain boundaries between adjacent plagioclase grains. Very few of these grain boundaries are parallel to growth faces of the plagioclase. Crossed polars with sensitive tint plate. Scale bar is 1 mm long.

partial melting. The first parts of the enclave to melt will be those with the lowest melting point and, in a fractionating system, these will be the last drops of the most evolved liquid. Gabbroic enclaves in the Skaergaard Campsite dyke demonstrate that partial melting begins at interstitial pockets filled with late-stage mineral assemblages, with melting extending to the albitic rims of the surrounding plagioclase primocrysts [10].

If ascent of the enclaves in the host magma is associated with significant exsolution and expansion of a volatile phase, the component grains of the enclave are likely to be pushed apart or broken. This will result in the creation of parallel-sided, vesicular, melt films on grain boundaries and in fractures: such late-stage features are easily distinguishable from the original, pre-entrainment, geometry of the melt-filled pores at depth.

7. Evidence for gravitationally driven compaction

Many authors have suggested that deep-seated crystal mushes collapse by viscous deformation driven by gravitational loading [50–56], leading to the formation of adcumulates at depth and the creation of large eruptible volumes of crystal-poor liquid [5]. It is generally assumed that the process of compaction occurs by viscous deformation of a crystal framework, in which the solid grains change shape via processes such as dislocation creep, dissolution–reprecipitation and melt-assisted grain boundary sliding: this viscous compaction is distinct from what can be termed 'mechanical compaction' [57], which is achieved by the re-arrangement of rigid, non-deforming, particles in the magmatic flow regime [58]. Mechanical compaction necessarily occurs at higher melt contents than viscous compaction and it is likely to be recorded by a strong shape-preferred orientation of grains that preserve no evidence of plastic deformation.

For viscous compaction achieved by dislocation creep, a high free dislocation density forms in response to the stress experienced by the system. Lattice misorientations (shown by undulose extinction and low-angle boundaries) are ubiquitous and (tapering) mechanical twins [58] are common (figure 4*a*). Extensive plastic deformation by dislocation creep results in a crystallographic preferred orientation, controlled by the slip systems active during deformation and a shape-preferred orientation that is required to accommodate the changes in volume during deformation. Dislocation creep is always accompanied by recrystallization, which annihilates dislocations or recovers them into sub-grains and grain boundaries (figure 4*b*) while the ongoing deformation continually generates new dislocations. Recrystallization will also remove evidence of any primary magmatic zoning. If the rock is cooled immediately after deformation, preventing static recrystallization, then the microstructures created during dislocation creep will be preserved. However, if the dislocation density in the crystals is sufficiently high and the system remains hot (greater than 500°C for plagioclase) after the cessation of deformation, recrystallization will continue under static conditions, erasing any shape-preferred orientation: the microstructure will become granular.

At low stress, the deformation required for viscous compaction occurs by diffusive processes. This is essentially pressure solution, driven by stress-induced chemical potential gradients whereby rock deforms via the diffusion of matter along grain boundaries, through a liquid phase or through the volume of grains [59]. This process is equivalent to diffusion creep, which is a grain size sensitive process and is always accompanied by grain boundary sliding [60]. Importantly, viscous deformation by a diffusion mechanism will not always leave a clearly identifiable microstructural record. Typical signatures of diffusion-controlled deformation are the truncation of grains of a known original shape, together with interpenetration of grains and the development of sutured contacts, and compositionally distinct overgrowths on faces oriented so that they are under relatively low stress [59–61]. However, apparently sutured grain boundaries can be created during primary solidification in the absence of deformation (see discussion below). Furthermore, highly irregular grain boundaries created during diffusion-controlled deformation are likely to become smooth during cooling, particularly between two grains of the same phase, driven by the reduction of interfacial energies [46,62].

Importantly, deformation by diffusive processes results in the partial or complete replacement of compositional zoning formed during the early stages of crystallization. Magmatic zoning is typically parallel to growth faces and strongly zoned mineral grains may contain a core recording their original shape. This provides the opportunity to identify any grain interpenetration by pressure solution. More generally, viscous compaction resulting in dissolution–reprecipitation will obliterate all grain boundaries defined by growth faces on primocrysts and create

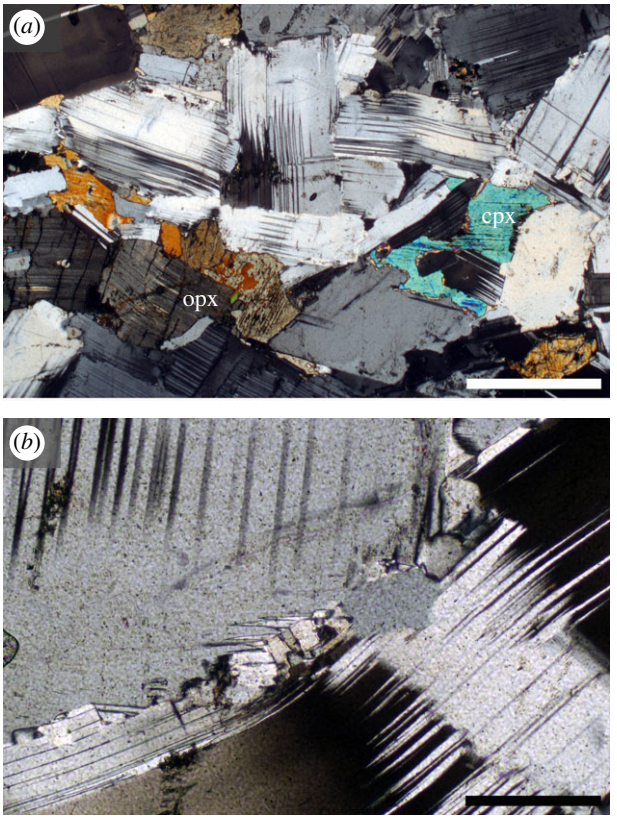

Figure 4. Cumulates from Middle Zone of the Rustenburg Layered Series of the Bushveld complex, South Africa. (*a*) Note the abundant tapering and curved deformation twins in the plagioclase and the irregular grain boundaries. Cumulus orthopyroxene grains are also bent although neighbouring interstitial clinopyroxene is not strongly deformed. Crossed polars. Scale bar is 1 mm long. (*b*) Grain boundaries between strongly deformed, original igneous, plagioclase grains are decorated with undeformed neoblasts that grew as a result of dynamic recrystallization. Crossed polars. Scale bar is 0.5 mm long.

discontinuities in the magmatic compositional zoning, associated with a localized loss of planar growth faces, particularly at high pressure points created where grains impinge at a high angle.

8. Microstructural evidence for crystal accumulation versus *in situ* growth

Crystallization regimes fall on a spectrum between an endmember in which solidification occurs on the margins of essentially crystal-free bodies of magma, in the manner certainly operating during solidification of the Skaergaard Intrusion, and another endmember represented by a hot mushy zone dominated by crystals in which any liquid-rich bodies of magma were small or short-lived. Microstructures can be used to distinguish between these two regimes.

Large bodies of essentially crystal-free magma, especially those with laterally extensive vertical walls, will generally convect, leading to mobilization and redistribution of crystals. Although convection in horizontal tabular bodies requires the critical Rayleigh number to be exceeded, cooling of magma at vertical walls will always create a gravitational instability that will drive convection on timescales shorter than that for crystallization if the liquid is not too viscous. As outlined above, it is straightforward to discern evidence for the large-scale convection indicative of a Skaergaard-style magma chamber from field observations. Although their small size and the absence of any spatial context means that we cannot use many of these field-based

criteria on entrained crystalline enclaves, we can use the microstructural understanding obtained from the study of exposed fully solidified bodies to make inferences about the crystallization regime in the enclave source.

With rare exceptions [26], enclaves and xenoliths are commonly too small to detect modal or grain size layering created by crystal re-arrangement in magmatic currents. However, particle re-arrangement in a liquid-rich convecting system commonly results in fabric formation defined by a shape-preferred orientation of non-equant grains. Unless subsequently affected by compaction, these grains show no evidence of deformation by either dislocation creep or a dissolution–reprecipitation mechanism. The microstructure in such rocks is characterized by planar growth faces on the mobilized grains and the juxtaposition of the mobilized grains so that these planar growth faces are in contact with no evidence for indentation. Further evidence in support of crystal accumulation, and hence crystallization of a liquid-rich magma body, is provided by a uniform grain size. Although a uniform grain size can be achieved in a closed system if solidification involved a single short burst of nucleation followed by crystal growth [63], in an open system in which crystals are mobile, a uniform grain size is consistent with hydrodynamical sorting (i.e. crystal redistribution and accumulation).

Grain boundary morphology provides an important discriminant of crystallization regime, being different in an environment in which grains are free to move relative to each other (i.e. a liquid-rich environment typical of a Skaergaard-style magma chamber) compared to the one in which crystals nucleate and grow in proximity (i.e. the situation expected for a liquid-poor crystal mush zone or the walls of a large magma chamber). Grains growing in a liquid-rich environment have a shape indicative of the relative rates of growth in different crystallographic directions and the symmetry of the crystal lattice. Minerals (such as plagioclase) that grow by birth-and-spread mechanisms are bounded by atomically smooth planar faces, whereas minerals that grow in some crystallographic directions by continuous attachment form grains with some areas of rounded melt–solid interface (e.g. quartz) [64,65]. Isolated grains suspended in a convecting magma form aggregate by synneusis, and these aggregates are typified by planar grain boundaries that are parallel to the growth faces of both grains (figure 3*e*). This can be clearly discerned if the grains are compositionally zoned [66,67]. By contrast, grain boundaries formed by the impingement of grains in a crystal-rich environment tend to be highly irregular, at random orientations to growth faces of the constituent minerals (figure 3*b*,*f*), with small pockets of melt (the impingement lenses of Holness *et al*. [34]) that are commonly pseudomorphed by other minerals during further solidification (figure 3*d*). Although irregular grain boundaries can be indicative of pressure solution [60,68], the presence of glass-filled impingement lenses demonstrates the primary growth origin of the irregularities.

Grain boundary morphology does not always provide unambiguous evidence about how they were formed, however, as shown by Means and Park who observed changes in grain boundary geometry by boundary migration in crystallizing, undeformed, samples of a synthetic analogue [69]. They observed that a boundary can change, during continued crystallization, from being euhedral with respect to one grain, to euhedral with respect to the other. No explanation was offered for this observation, but similar behaviour in clusters of silicate grains can potentially be detected using compositional zoning to detect successive growth phases. In the absence of firm evidence supporting a changing boundary morphology during growth, an assessment of the relative importance of the two types of grain boundary should reveal the timing and extent to which the enclave grew in a hot mush zone or on the margins of a large liquid-rich magma chamber.

(a) Distinguishing the location of crystallization in a liquid-rich magma body

Critically, the solidification of a magma chamber may involve the inwards growth of mushy layers on vertical walls as well as accumulation of material at the (sub-) horizontal floor and roof. The microstructures developed in these three environments will be different: is it possible to find

microstructural (or geochemical) criteria by which the growth environments can be distinguished from each other as well as from that in a long-lived crystal mushy zone?

The best natural laboratories in which to develop the necessary microstructural criteria are layered intrusions. The Eastern Layered Intrusion of Rum, Inner Hebrides of Scotland, had no vertical walls and was most probably sill-like for much of its life [70]. By contrast, the Skaergaard Intrusion is box-like with walls approximately 4 km high [7,71]. Crystal mushy layers developed on the walls, floor and roof of the Skaergaard, with solidification involving the inwards-propagation of all three. While the gabbroic cumulates formed on the floor of the Skaergaard Intrusion (the Layered Series) have many features in common with the troctolites and gabbros of the Rum Eastern Layered Intrusion, the microstructures in the rocks from the vertical wall (the Marginal Border Series) are distinctly different.

Fabrics are common in both the magma chamber floor cumulates of the Rum Eastern Layered Intrusion and the Skaergaard Layered Series and are predominantly defined by a shape-preferred orientation of 'roughly square' tablets of plagioclase flattened parallel to (010), bounded by planar growth faces [7,14,72] (e.g. figure 1*a*). In Skaergaard, magmatic foliations together with evidence for shearing (grain tiling, grain imbrication, oblique foliation) led Nicolas [58] to argue that the fabrics result from grain orientation in currents flowing from the walls onto an already consolidated floor [57]. At high stratigraphic levels, plagioclase forms laths that are elongate along [100] [73,74]: these are preferentially oriented to define a lineation in sedimentary features known as trough layers, in which the lineation is parallel to the likely direction of flow of crystal-laden magmas [7,14,72–75].

Despite the relative proximity of the intrusion margins, the inner parts of the Skaergaard Marginal Border Series are commonly coarser-grained than equivalent rocks of the Layered Series. All regions of the Marginal Border Series are characterized by a wider range of grain sizes in any one sample compared to stratigraphically equivalent cumulates of the Layered Series (figure 5). There is no evidence for any preferred orientation of either crystallographic orientation or grain shape in the Marginal Border Series; neither is there any evidence of intragrain deformation. The randomly oriented plagioclase grains commonly have irregular and sutured mutual grain boundaries (figure 3*f*). Interstitial material is abundant and normal zoning of individual mineral grains is common (figure 5*b*), indicating significant amounts of interstitial overgrowth from a continuously evolving melt [9]. The evolved rims of constant composition that are a feature of plagioclase grains in the lower parts of the Layered Series are absent in the Marginal Border Series [9]. In contrast to the Layered Series, the Marginal Border Series contains none of the reactive symplectites that have been attributed to differential migration of immiscible interstitial liquids, with the loss of the buoyant Si-rich immiscible conjugate triggering a reaction between the remaining dense Fe-rich conjugate and the surrounding primocrysts [76].

These distinctive characteristics of Marginal Border Series rocks can be attributed to the vertical orientation of the wall. The absence of reactive symplectites is because, at any point in the wall, the rising buoyant Si-rich conjugate is replaced by the Si-rich liquid of the same composition from the underlying mush: the Si-rich conjugate can only be lost by lateral flow for which there is no driving force. The absence of constant composition rims on plagioclase grains, together with the relative enrichment in interstitial liquid, points to a strongly orthocumulate status. The absence of preferred grain alignment and a wide range of grain sizes is consistent with an absence of particle re-arrangement by magmatic currents (because, on a vertical wall adjacent to crystal-poor liquid, any crystals sufficiently poorly bound to their neighbours to be re-arranged will simply be removed rather than aligned). The wide range of grain sizes, together with the irregular plagioclase–plagioclase grain boundaries, is also consistent with continuous *in situ* heterogeneous nucleation and growth. We would expect similar features to be present in crystal mushes grown on the walls of vertical conduits: additionally, since narrow conduits are likely to cool quickly, any conduit mushes will be fine-grained.

Roof cumulates are necessarily formed either by *in situ* nucleation and growth or by the accumulation of buoyant minerals and grain clusters. Interstitial liquid that is denser than the underlying liquid will be lost from a permeable roof cumulate, while a buoyant liquid will

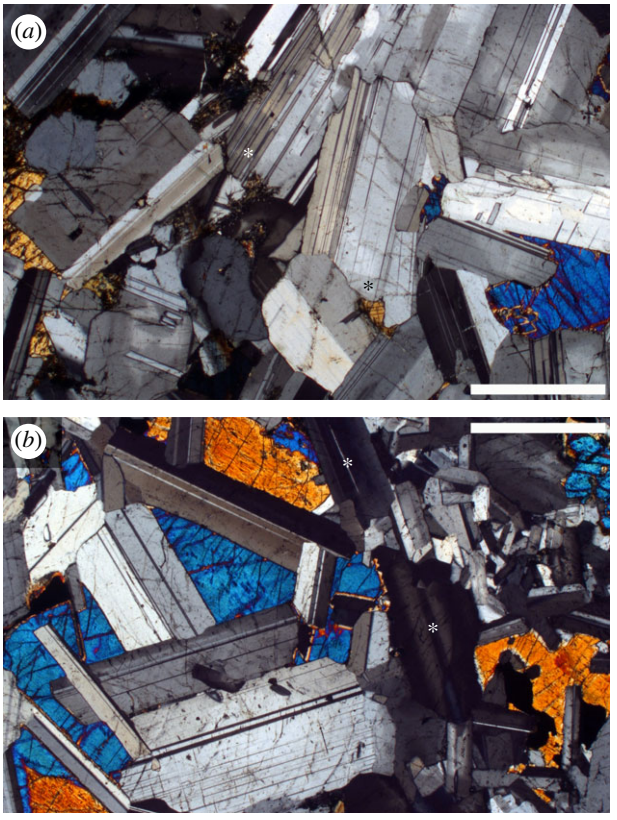

Figure 5. Sample 458220 from Lower Zone (LZa) of the Skaergaard Layered Series, in which plagioclase is cumulus and augite in interstitial. Note the small range in plagioclase grain sizes and the wide constant composition relatively albitic rims (examples are marked with an asterisk). This sample has only a very weak fabric. Crossed polars. Scale bar is 1 mm long. (*a*) Sample from the LZa equivalent in the Marginal Border Series. Note the wide range of grain sizes of the plagioclase and the abundant normal zoning (examples are marked with an asterisk). Crossed polars. Scale bar is 1 mm long.

be retained. Although microstructures of roof cumulates have not been studied in detail, some generalizations can be made about their nature from observation of well-exposed examples in the Skaergaard Intrusion.

The Skaergaard roof cumulates have a generally more silicic bulk composition than their temporal equivalents on the floor and walls [77,78]. They contain relatively more plagioclase (which is buoyant in the Skaergaard liquid), and abundant interstitial granophyre (thought to have crystallized from the Si-rich conjugate of an unmixed interstitial liquid [76]). There are none of the ilmenite-rich intergrowths that record the crystallization of pockets of interstitial Fe-rich liquid, suggesting that this dense immiscible conjugate was lost from the roof. The roof cumulates are generally strongly orthocumulate, with abundant late-stage minerals such as apatite [6,77]. Fabrics, such as lineations and foliations, are not common, but where present are defined by plagioclase [7]: all other primocryst minerals are denser than the remaining liquid, so re-organization by magmatic currents sweeps them away from the roof. None of the dense phases show the mono-disperse grain size distributions expected for minerals that underwent hydrodynamic sorting, suggesting they grew *in situ*. There is no evidence of plastic deformation, suggesting that viscous compaction (which can only be driven by the upwards gravitational force associated with plagioclase buoyancy) does not occur.

Although it might not be straightforward to distinguish enclaves derived from the walls of a liquid-rich magma chamber from those derived from a solid-dominated crystal mushy zone, were

an eruption sampling a magma chamber, one would expect the suite of enclaves to include at least some examples with microstructural characteristics of either a floor or a roof accumulation.

9. Analytical methods

QEMSCAN images were obtained for the Rábida enclaves using a Quanta 650 F field emission gun scanning electron microscope (SEM), equipped with two Brucker XFlash 6130 energy-dispersive spectrometers (EDS), at the Department of Earth Sciences, University of Cambridge. QEMSCAN images were collected with a 7.5 µm pixel resolution. For further information on the analytical procedure, see Holness [49]. The QEMSCAN images were used to create phase maps and maps of Ca concentration, to enable easy visualization of compositional zoning in plagioclase.

10. Case study 1: the Kameni Islands, Santorini

The Kameni Islands comprise dacitic lavas erupted in the centre of the Santorini Volcano caldera, which formed during the Minoan eruption 3600 years ago [79]. The exposed rocks on the Kameni Islands record at least nine subaerial eruptions, the last of which formed a dome in 1950. The pre-1950 lava flows contain a variety of crystal-rich glassy mafic enclaves, the majority of which are andesitic. These are interpreted to be the remnants of a layer of replenishing magma that ponded at the base of a magma chamber, which was disrupted and overturned immediately prior to each eruption [80]. The 1950 lava dome also contains these glass-rich andesitic enclaves, which range in size up to 20 cm in diameter, but is unique in containing a significant number of much smaller, almost wholly crystalline, enclaves of cognate troctolitic or gabbroic material (which are present, albeit very rare, in the earlier flows). The following discussion focuses entirely on this latter group of enclaves, which are coarse-grained (grain size up to 1 mm), with a low glass and vesicle content, and with a maximum diameter of 5 cm [34]. They are sub-rounded to angular and many are often enveloped in less dense, highly vesicular crystal-rich material similar to that of the more common type of andesitic enclaves. They are interpreted as fragments of a deep crustal crystal mush.

The gabbroic and troctolitic enclaves from Kameni are dominated by plagioclase, with primocrysts of olivine ± pyroxene. They contain clusters of rounded olivine (±clinopyroxene) grains, characterized by planar grain boundaries parallel to the common growth faces of olivine (figure 6*a*), similar to those found in the Shiant Isles Main sill and ascribed to cluster formation by synneusis of crystals suspended in a convecting magma [8]. The enclaves preserve no evidence for primary igneous shape-preferred orientations and the plagioclase is notably equant (figure 6*b–e*). Although there are too few grains in each of these small enclaves to obtain meaningful values for AR, the clearly low aspect ratios contrast with those of plagioclase erupted as phenocrysts in the host lava or in the associated abundant andesitic enclaves, and are consistent with much slower crystallization rates for the gabbroic/troctolitic enclaves [44].

There is localized evidence for melt–solid–solid textural equilibration, particularly at olivine–olivine–melt junctions (figure 6*f*), with some limited evidence at plagioclase–plagioclase junctions (figure 6*b*,*c*,*f*), consistent with relatively slow crystallization rates. Some plagioclase–plagioclase–melt junctions have been modified during or after entrainment, with evidence for late-stage rapid growth resulting in the creation of irregular, but curved, plagioclase–melt interfaces [81] (figure 6*d*,*f*).

The margins of plagioclase grains are strongly facetted where they are growing into relatively large melt pools (figure 6*c–f*). Grain boundaries between adjacent plagioclase grains are a mixture of planar boundaries that are parallel to growth faces of one or both of the two grains (e.g. figure 6*b*,*e*), or are irregular, with no relationship with the crystallographic orientation of the two grains. This irregular type contains impingement lenses (figure 6*c–e*). That the irregularities in the grain boundaries formed during solidification itself is shown by the fact that planar facets are present on plagioclase grains adjacent to relatively large pools of melt, but this planar morphology breaks down as the melt film between adjacent grains is narrowed during continuing

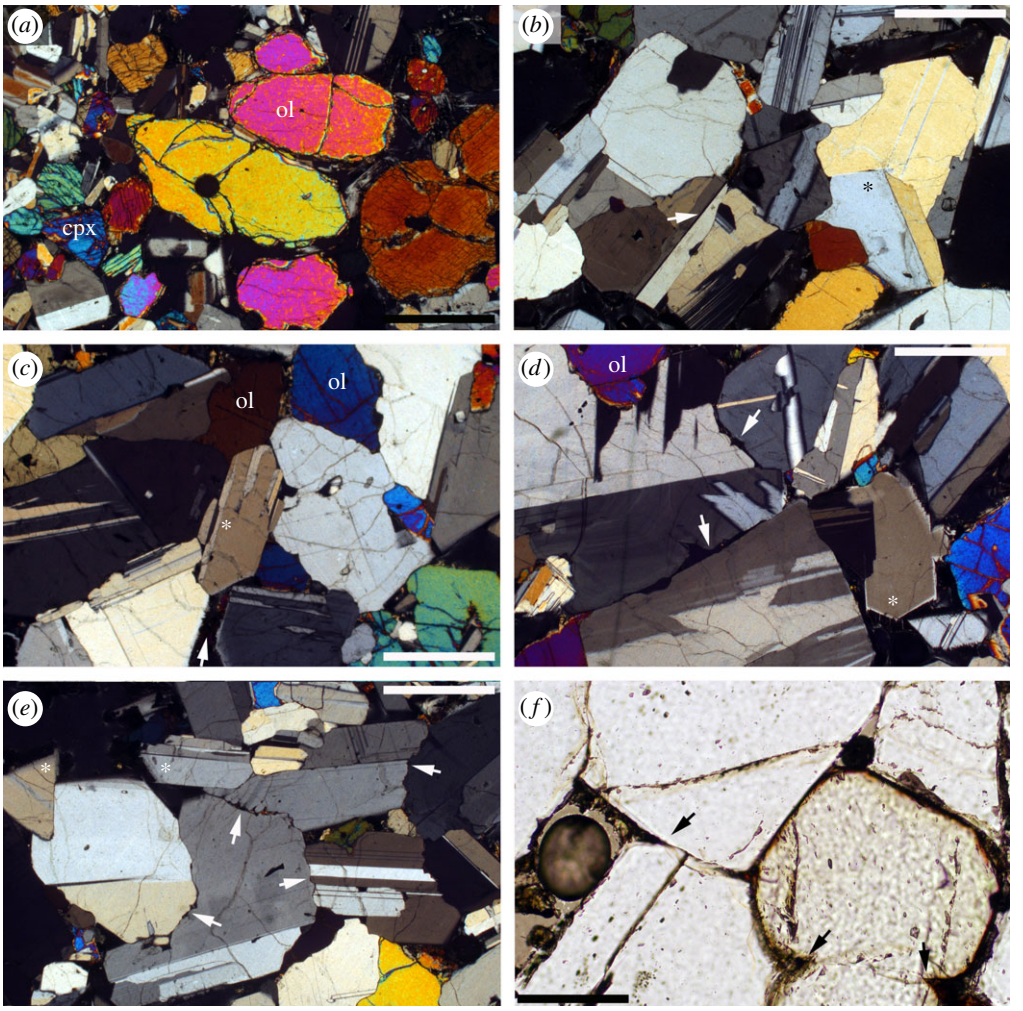

Figure 6. Troctolitic and gabbroic glass-bearing enclaves entrained in the 1950 andesite flow of the Kameni Islands, Santorini. (*a*) Clusters of euhedral to subhedral olivine and augite grains, joined by large areas of planar grain boundary consistent with a formation during synneusis. Crossed polars. Scale bar is 1 mm long. (*b*) Plagioclase grains in this enclave have low aspect ratios, commonly with complex twinning, and no evidence for dislocation creep (the yellow birefringence colour is due to the thickness of this thin section). The arrowed grain boundary is planar, melt-free and joins two plagioclase grains on their (010) faces: this is suggestive of sintering following synneusis. The grain marked with an asterisk is joined by similarly straight, (010) parallel grain boundaries to adjacent grains. Crossed polars. Scale bar is 1 mm long. (*c*) While many plagioclase grains have low AR, some are more elongate, with evidence of sintering following synneusis (grain marked with an asterisk). Note the planar growth faces where plagioclase is adjacent to large pockets of melt (example is marked by an arrow). Crossed polars. Scale bar is 1 mm long. (*d*) The grain marked with an asterisk has planar growth facets where it protrudes into a large melt-filled pocket (note the serrated, pale grey margins—these grew rapidly after entrainment). The two arrows show the location of wide melt-filled boundaries bounded by highly irregular plagioclase growth faces. Continued growth of these grains will result in the trapping of residual melt to form impingement lenses. Crossed polars. Scale bar is 1 mm long. (*e*) The two white arrows on the left denote wide melt films on developing grain boundaries between plagioclase grains, whereas those on the right show the location of highly irregular grain boundaries formed by impingement growth. Crossed polars. Scale bar is 1 mm long. (*f*) The rounded olivine grains have low dihedral angles where in contact (arrowed) denoting some approach to textural equilibrium at pore corners. There is rather less evidence of textural equilibration at plagioclase–plagioclase junctions, with some rounding caused by diffusion-limited late-stage growth during quenching (an example on the left of the image is arrowed—note the clearly defined smooth inner surface of the overgrowth rim compared with the more irregular outer surface adjacent to the interstitial quenched glass [81]). Plane polarized light. Scale bar is 0.5 mm long.

solidification. The irregular boundaries are therefore a consequence of the infilling of melt-filled space by the progressive growth towards each other of two motionless grains.

What can we deduce about the extent to which melt may have been extracted from the crystal mushy source of these enclaves? They record no evidence for dislocation creep, with no distorted grains or evidence of sub-grains (figure 6): there is no evidence of viscous compaction. Any melt extraction must therefore have occurred only by diffusive mechanisms, which primarily involve melt on grain boundaries. The planar grain boundaries in the enclaves do not contain optically resolvable melt films and are unlikely to have played a role in either diffusion-reprecipitation creep or melt-assisted diffusion creep. By contrast, the irregular nascent boundaries forming between adjacent grains that are growing towards each other do contain melt: their irregular geometry may have provided high-stress contacts for dissolution, but there is no optically visible evidence for high dislocation densities at these points. Furthermore, melt-assisted creep during compaction would reduce grain boundary irregularity and one might therefore expect a preferred orientation of straight boundaries, reflecting the stress field during compaction: no evidence for this is present, although the enclaves are perhaps too small for a detailed assessment. In summary, there is no good evidence for melt extraction from the mushy source of these enclaves—future work exploring this question should be focused on larger specimens of incompletely solidified mush in order to detect any preferential orientation of planar versus irregular grain boundaries.

The microstructural evidence preserved in the Kameni gabbroic and troctolitic enclaves suggests that the crystal mushy zone they came from was built progressively by the accumulation of grain clusters (comprising all three primocryst phases) formed by synneusis. Although synneusis is indicative of a melt-rich environment, once the clusters had accumulated to form a mush, this was not then reworked by magmatic currents or other deformation of the mush pile, perhaps indicative of a small non-convecting magma chamber. The low AR of the plagioclase indicates a slow cooling rate, but this was still sufficiently fast to prevent the geometry of the remaining plagioclase-bounded melt-filled pores to be controlled by minimization of interfacial energies: we await a quantitative understanding of textural equilibration rates to place firm constraints on the cooling rate (and hence size) of the magma source region. It is unlikely, on the basis of the evidence presented here, that any melt was extracted from the crystal mush. The small size of the gabbroic and troctolitic enclaves and their comparative rarity, particularly in comparison with the much more abundant andesitic enclaves in the Kameni lavas, suggests that entrainment was not as straightforward as those of the associated highly abundant andesitic enclaves. We suggest that they were probably sourced from a deeper body, with their small size and rarity due to the difficulty in erupting material from levels deeper than the shallow chamber that fed the eruptions.

11. Case study 2: Rábida volcano, Galápagos

Rábida volcano forms one of the smallest major islands in the Galápagos Archipelago. It is constructed of a diverse suite of rocks, ranging from primitive olivine-basaltic lavas through icelandite domes to a rhyodacitic ignimbrite. An arcuate fault on the western part of the island strikes NNW and could be the remnants of a mostly buried caldera [82]. Potassium-argon ages of exposed rocks are all within 1.0 ± 0.1 Ma [83].

We collected a suite of 11 plagioclase-rich cumulate-textured enclaves from a wave-dissected scoria cone on the north coast of the island. The scoria and ash making up the cone have a distinctive red coloration, probably due to limited interaction with seawater during eruption, intermediate in style between Strombolian and Surtseyan. Most of the enclaves are coated with a rind of quenched scoria, but some are isolated rocks with none of the carriers in direct contact. The enclaves range in size up to approximately 10 cm in diameter. Some are round cobbles, and others have planar margins consistent with a formation by the fracturing of the source.

The suite of 11 enclaves is dominated by plagioclase tablets with a generally low average AR (as viewed in thin section), in the range 1.67 ± 0.8 to 2.59 ± 0.15. There is a wide range of lithologies, encompassing relatively primitive troctolitic compositions to enclaves containing

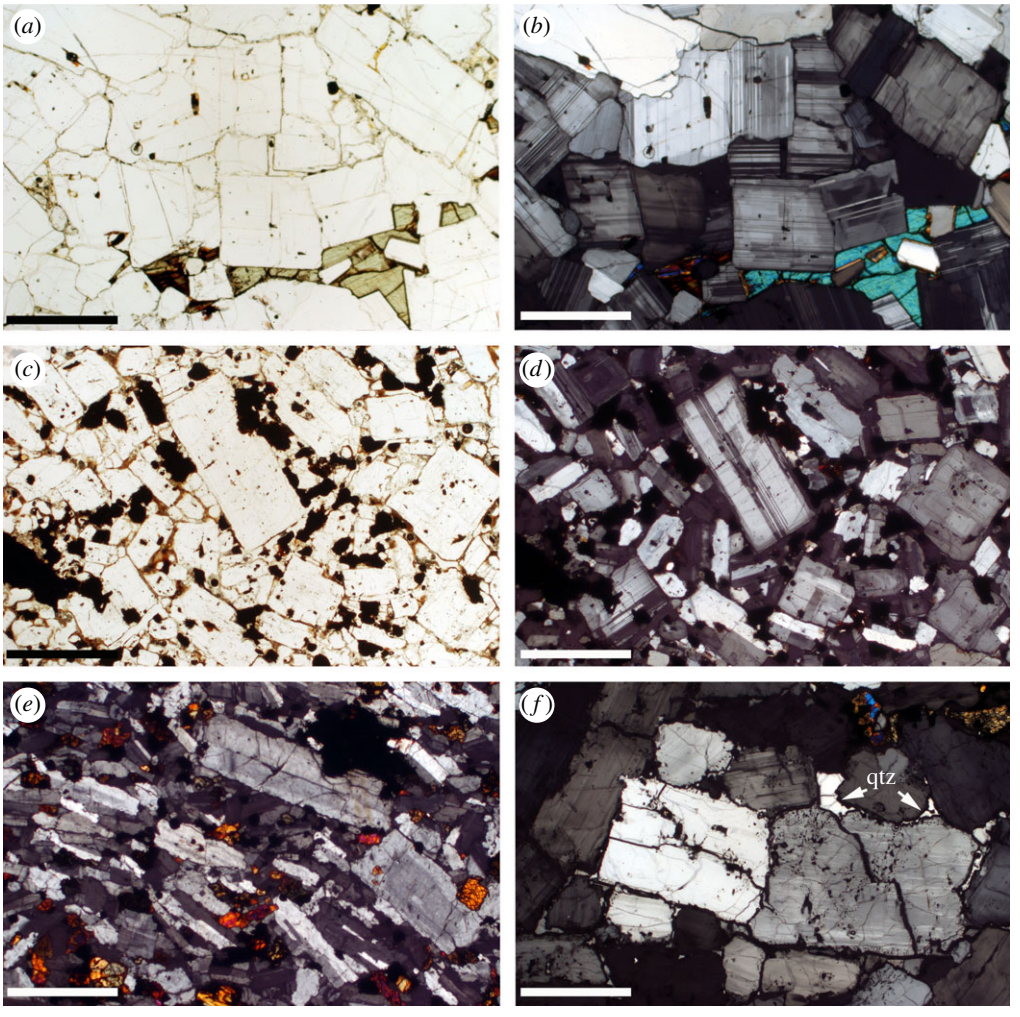

Figure 7. Photomicrographs of the Rábida enclaves, Galápagos. (*a*) Plagioclase-rich enclave, with interstitial clinopyroxene and vesicular glass, photographed under plane polarized light. (*b*) shows the same area photographed under crossed polars. Note the absence of preferred orientation of the euhedral, low AR, plagioclase grains, their uniform grain size, and the frequency with which grain boundaries are formed by the juxtaposition of planar growth faces. Scale bar in both images is 1 mm long. (*c*) Plagioclase-rich enclave, with abundant small rounded grains of oxide and interstitial vesicular glass, photographed under plane polarized light. (*d*) shows the same area photographed under crossed polars. The range of grain sizes in this enclave is large, and the larger grains are commonly normally zoned. Note the evidence for complex zoning, with other grains apparently not zoned at all. The scale bar in both images is 1 mm long. (*e*) A strong preferred orientation of relatively elongate plagioclase. Note the scattering of small equant clinopyroxene grains. Crossed polars. Scale bar is 1 mm long. (*f*) Euhedral, equant plagioclase grains are separated by irregular but parallel-sided voids, with some transgranular fractures. The grain boundary voids are likely to have been created by decompaction caused by devolatilization of interstitial melt during ascent. Note the interstitial quartz (labelled qtz; examples are arrowed), which is also separated from the adjacent plagioclase by parallel-side voids. Crossed polars. Scale bar is 1 mm long.

primocrysts of clinopyroxene, oxides, amphibole and abundant apatite. Where present, olivine forms rounded grains (many are strongly oxidized).

A microstructural progression, based on plagioclase morphology, is suggestive of progressive fractionation. The most primitive enclaves contain an abundance of euhedral plagioclase grains, comprising 60–95 vol.% of the mode. The grain size is commonly mono-disperse in any one

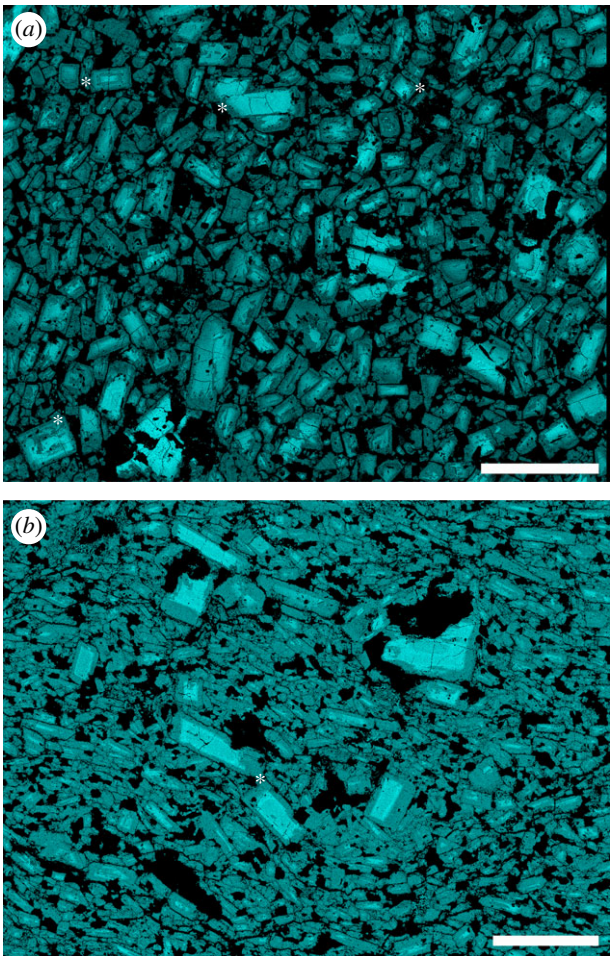

Figure 8. QEMSCAN images highlighting the Ca content of plagioclase in the Rábida enclaves, Galápagos. Bright colours denote high Ca content and the darker teal more albitic compositions: phases other than plagioclase are black in these images. (*a*) Same enclave as depicted in figure 7*c*,*d*. Note the presence of several different zoning patterns, with particular examples of either normal, patchy or oscillatory zoning marked by asterisks. It is not possible to reproduce this range of apparent zoning types by sectioning through a single type. Scale bar is 2 mm long. (*b*) Same enclave as depicted in figure 7*e*. The two large plagioclase grains either side of the asterisk are the two larger grains shown in figure 7*e*. Note the strong preferred orientation. The relatively larger grains in this field of view have strongly calcic cores, in contrast to the majority of the smaller grains which have complex partially resorbed cores attesting to a different growth history. Scale bar is 2 mm long.

enclave, in the range 0.2–2 mm (figure 7*a*,*b*), but a few of the finer-grained enclaves contain small numbers of grains that are significantly larger than the rest (figures 7*c*–*e* and 8). The plagioclase grains in most of our sample suite are randomly oriented (figure 7*a*–*d*) with few clusters joined by planar boundaries parallel to growth faces. The plagioclase in one enclave is strongly aligned to form a foliation (figures 7*e* and 8). Plagioclase grains within a single enclave show a range of compositional zonation, with some grains apparently unzoned and others with either normal, oscillatory or patchy zoning (figures 7*d* and 8). Subordinate quantities of euhedral grains of clinopyroxene (figure 7*e*), oxides (figure 7*c*,*d*) or olivine may also be present. Clinopyroxene (figure 7*a*,*b*) and quartz (figure 7*f*) may be interstitial phases, and up to 10 vol.% of these enclaves is occupied by glass or voids.

The morphology of the plagioclase margins varies from planar to highly irregular. In enclaves with planar plagioclase margins, the spaces between these euhedral grains are filled with either

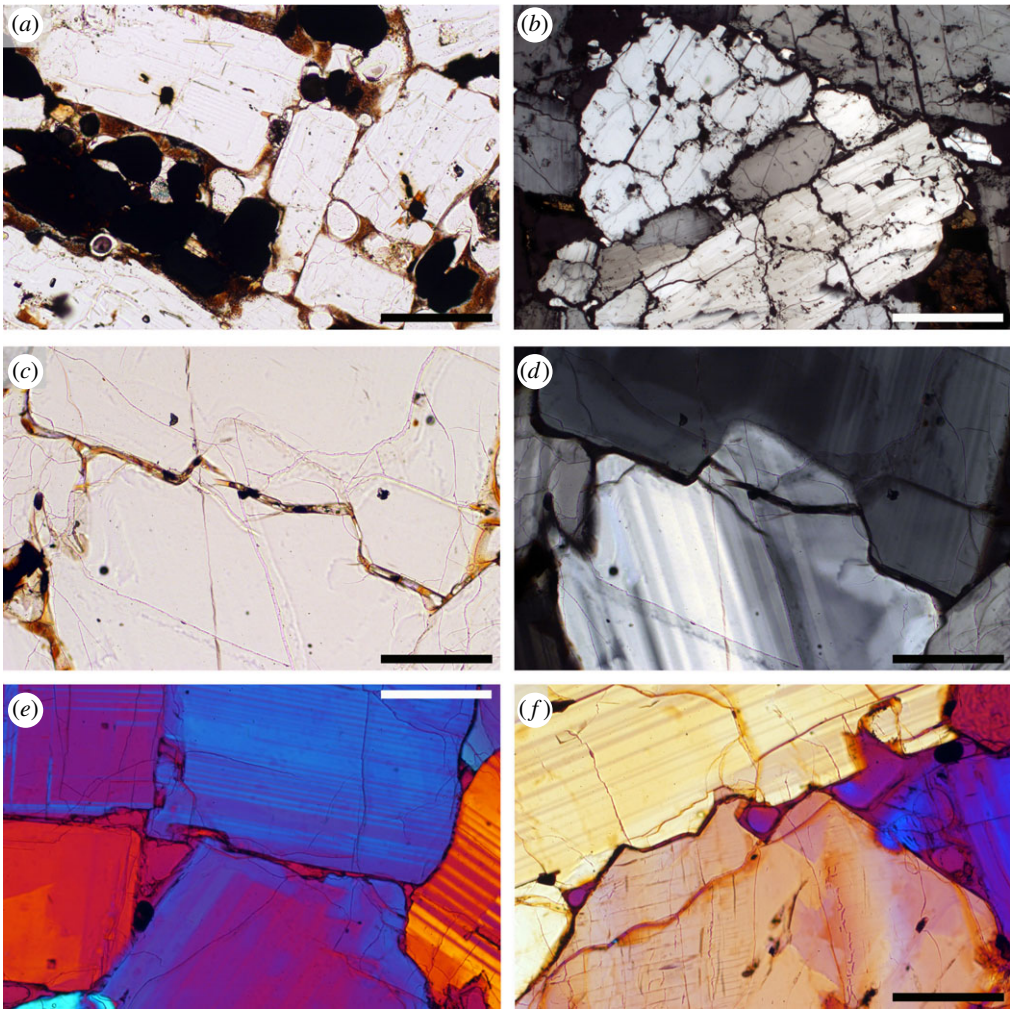

Figure 9. Photomicrographs of the Rábida enclaves, Galápagos. (*a*) Euhedral plagioclase and rounded grains of Fe–Ti oxides, set in highly vesicular interstitial glass. Plane polarized light. Scale bar is 0.5 mm long. (*b*) All grain boundaries in this enclave have been opened and are now either voids or locally contain some vesicular glass. Note the abundant interstitial quartz. Crossed polars. Scale bar is 1 mm long. (*c*) A grain boundary containing vesicular glass separates two plagioclase grains, photographed under plane polarized light. The same area is photographed under crossed polars in (*d*), in which it is apparent that the grain boundary has been opened by decompaction caused by devolatilization during ascent, as the newly opened fracture also cuts one of the plagioclase grains. Scale bar in both images is 0.5 mm long. (*e*) Interstitial pockets of vesicular glass are bounded by either planar plagioclase growth faces (with localized limited approach to texturally equilibrated dihedral angles) or form impingement lenses along grain boundaries. Crossed polars with a sensitive tint plate. Scale bar is 0.5 mm long. (*f*) Irregular grain boundary between two plagioclase grains, containing vesicular glass. Crossed polars with a sensitive tint plate. Scale bar is 0.5 mm long.

vesicular glass (figure 9*a*) or interstitial clinopyroxene or quartz (figures 7*a*,*b*,*f* and 9*b*). In enclaves with highly irregular plagioclase margins, grain boundary voids and melt films are abundant. Irregular plagioclase margins fall into two types: one is a jigsaw-fit geometry, where grains can be fit together by closing the voids (figures 7*f* and 9*b*). This type is associated with intragrain fractures (figure 7*f*), which are locally occupied by glass (figure 9*c*,*d*) and is clearly a consequence of decompaction driven by vesiculation of the interstitial liquid during ascent. The other type is characterized by non-parallel-sided and discontinuous impingement lenses (figure 9*e*,*f*).

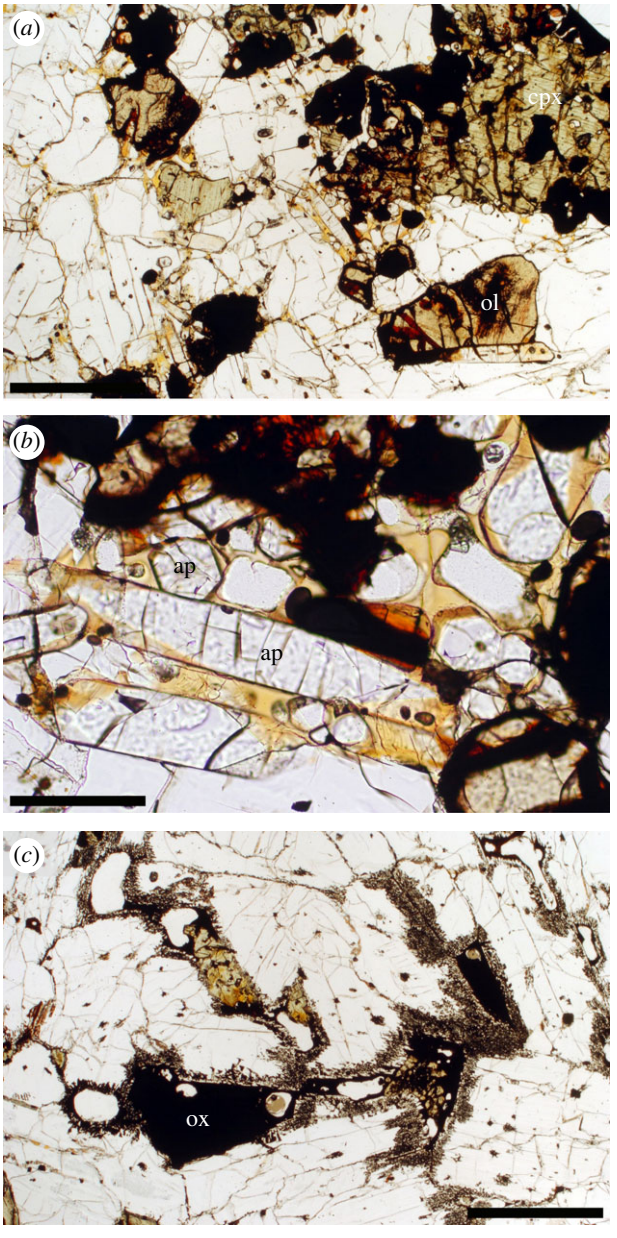

Figure 10. Photomicrographs of the Rábida enclaves, Galápagos. (*a*) Enclave containing primocrysts of plagioclase, clinopyroxene, Fe–Ti oxides, with abundant apatite. The central part of this image is magnified in (*b*) Plane polarized light. Scale bar is 1 mm long. (*b*) Primocrysts of apatite (labelled ap) are concentrated in, or adjacent to, pockets of glass, demonstrating that they crystallized relatively late. Plane polarized light. Scale bar is 0.5 mm long. (*c*) Plagioclase adjacent to pockets of (oxidized) glass or minerals that arrive relatively late on the liquidus has developed a sieve texture consistent with partial melting of the most evolved (and hence with the lowest temperature of crystallization) regions of the enclave during entrainment and ascent in a relatively hot magma. Plane polarized light. Scale bar is 1 mm long.

More evolved enclaves, while still rich in plagioclase (40–50 vol.%), are characterized by an abundance of large primocrysts of clinopyroxene, amphibole and oxides with subordinate fayalitic olivine (figure 10*a*). Apatite and zircon are abundant. The proportion of glass varies from a few vol.% to 10 vol.%, and apatite is commonly concentrated in, or adjacent to, pockets

of glass (figure 10*a*,*b*). The four enclaves in this category have no preferred orientation of the elongate grains. The plagioclase grains locally develop a sieve-like texture where adjacent to melt pools (figure 10*c*), indicative of partial melting during/after incorporation into a hotter entraining magma.

There is no evidence of deformation in any of the enclaves, irrespective of either the extent of solidification or modal composition. The abundance of voids on grain boundaries prevents a detailed assessment of three-grain junction geometry, but the preserved corners of glass-filled pores are consistent with a morphology controlled by crystal growth kinetics rather than by the minimization of interfacial energies.

Our observations are consistent with the growth of essentially isolated crystals in a liquid-rich environment followed by accumulation to form a porous mush in which further solidification occurred on the now motionless grains in the mush pile. The rarity of preferred orientations of non-equant grains suggests that reworking of the accumulated crystals by magmatic currents was rare. However, reworking of low AR grains is not expected to create a strong fabric and, indeed, the single enclave with high AR plagioclase does have a shape-preferred orientation. The mono-disperse grain size distribution in many of the enclaves is suggestive of significant hydrodynamic sorting and points therefore to reworking of crystal accumulation by magmatic currents. The absence of much evidence for synneusis is intriguing and suggests that the growing grains (particularly plagioclase) did not encounter other grains before final accumulation. The crystal accumulation underwent no discernible deformation that would have resulted in the expulsion of interstitial liquid: there is no evidence of viscous compaction.

The microstructures point to the presence of liquid-rich magma bodies beneath Rábida volcano, in which marginal crystal accumulations formed, either by flotation or by settling. The mono-disperse grain size distribution and the frequency of non-touching contacts demonstrate that there was no significant heterogeneous nucleation that is an essential component of building a mushy layer on a vertical wall. The marginal crystal accumulation must therefore have formed on the floor or roof of these liquid-rich magma bodies.

The wide range of zoning types present in any one enclave is consistent with the accumulation of crystals from a wide range of different sources. The same range of zoning types is present in porphyritic Rábida basalts, suggesting that the assembly of a mixed cargo of crystals from a range of sources is important both during the history of a liquid-filled magma chamber and during the transport of magma to the surface. The microstructural evidence for large liquid-rich magma bodies preserved in the enclaves shows that a mixed crystal cargo in erupted magma cannot be taken in isolation as evidence for the development of a large sub-volcanic mushy zone by the amalgamation of multiple sills. Using the correlation of Holness [44], the AR of the plagioclase in the Rábida enclaves translates into crystallization timescales of 130–2300 years. Taking these timescales to be the thermal time constant (the time taken for a thermal difference to decay to $1/e$ of its original value) of the magma body in which the plagioclase crystallized indicates magma bodies of dimensions in the range 100–800 m. This is within the range of magma body size estimated on the basis of eruptive history and geochemical variations at Wolf and Ecuador Volcanoes, which range from 50 to 800 m thick at Wolf [84] and 120 m thick at Ecuador [85]. It is also consistent with the geophysical and petrologic syntheses that have led to a model of melt-rich sills hosted in a crustal-scale cumulate mush column [86,87].

12. Conclusion and directions for future work

Clear microstructural differences characterize plutonic rocks which formed in a dynamic liquid-rich environment, in which crystals can be moved and re-arranged by magmatic currents, and those in which crystal nucleation and growth are essentially *in situ* and static. Identifying these regimes in the magma plumbing systems beneath volcanoes is essential for determining the existence of magma chambers *sensu lato* and testing the spatial and temporal ubiquity of the recent trans-crustal mushy zone paradigm. We have shown that, by applying techniques developed

on intrusive rocks, microstructural observations of exhumed crystalline enclaves can act as an effective discriminant.

Crystals in samples of deep-sourced material from both the Kameni Islands of Santorini and Rábida Volcano in the Galápagos preserve evidence of genesis in a liquid-rich environment. The Kameni enclaves appear to record an early stage during which crystals were free to move, with the bulk of crystallization occurring in a static, mushy environment. By contrast, the source of the Rábida enclaves was an environment in which hydrodynamic sorting and re-arrangement by magmatic currents were common, consistent with a liquid-rich magma chamber. None of the enclaves from either volcano preserve evidence of compaction.

A point which has not been addressed in this paper and requires significant further work is the perhaps semantic question of how big does a magma body need to be before it can be termed a 'magma chamber'. We have discussed four crystallization environments: the floor of a volume of crystal-poor magma, at which crystals are mobilized and accumulate from elsewhere; the roof of a crystal-poor magma chamber in which some crystal accumulation occurs, together with *in situ* nucleation and growth; the walls of a crystal-poor magma volume, which solidify only via *in situ* crystal nucleation and growth; and mushy zones, in which crystallization is only *in situ*. The relative importance of these three environments depends not only on magma viscosity (and hence composition) but also on the geometry of magma bodies, their size and the timing and volume of any magma replenishments. How large or undisturbed does a magma body need to be in order to exhibit the various microstructural characteristics discussed in this contribution? For example, what would be the crystallization regime in a small lens of crystal-poor melt hosted in a larger mush zone? Refining the ideas presented here should be the target of future work.

There is much scope for further work on the microstructural evolution of sub-volcanic mush. An important question needing to be addressed concerns the importance of magma viscosity in controlling the fluid dynamical behaviour and hence the crystallization regime of magma bodies. We have concentrated on mafic systems, but the fluid dynamical behaviour of a more viscous silicic system, in which there is generally a smaller density difference between solids and liquid, will be very different. Laminar flow is almost certain to dominate [88,89]: the well-documented examples of modal layering in silicic bodies [90], strongly reminiscent of those in the mafic Skaergaard Intrusion, are unlikely to have identical microstructures, reflecting the very different flow regime during their formation.

The separation of melt from cumulates remains one of the most outstanding questions in igneous petrology, and there is a near absence of microstructural evidence for compaction in the natural record. Although there is overwhelming evidence that fractionation by the separation of crystals and residual liquid is responsible for the compositional diversity of both cumulates and melts in systems ranging from basaltic to silicic, the mechanism by which differentiated melt is extracted from the mush pile is unknown. Future work should be focused on solving this problem.

Quantification of the prevalence of many of the features we have described in this contribution, such as planar versus non-planar grain boundaries, grain boundary orientations relative to crystallographic orientations, and the strength of shape-preferred orientations relative to the shape of the constituent grains, is needed in order to place tighter constraints on the crystallization regime in which they formed, with a particular focus on the relatively neglected rocks that form on the upper surfaces of magma bodies. What is also currently missing from our toolbox is a reliable quantitative speedometer based on the extent of textural equilibration in both the super- and the sub-solidus. Experimental work should focus on the determination of the rates at which equilibrium dihedral angles can be attained, in order to place constraints on the cooling rate (and hence size) of the deep crustal magma bodies sampled by enclaves. Similarly, if we had a quantitative understanding of the rates at which textural equilibrium can be attained in fully solidified rocks, we could 'read through' any microstructural overprint on ancient plutonic rocks to decode their solidification history, for example, in the exhumed roots of ancient volcanic systems.

Finally, the observations described here demonstrate that there are systematic characteristics of melt distribution in partially solidified silicate rocks. At present, we have little understanding

of how variations in permeability and porosity in natural examples affect the response of partially solidified materials to seismic waves or electric and magnetic currents: coupling careful observation of the melt distribution to their geophysical response is key to accurate interpretation of the geophysical signals of deep-seated regions of partial melt.

Data accessibility. This article has no additional data.

Authors' contributions. M.B.H. carried out microstructural investigations and wrote much of the main text, M.S. carried out QEMSCAN and microstructural analysis and D.G. interpreted the Galápagos results in terms of the volcanic history.

Competing interests. We declare we have no competing interests.

Funding. M.B.H. acknowledges support from the Natural Environment Research Council (grant nos. NE/N009894/1 and NE/M013561/1). M.J.S. received support from a Charles Darwin and Galápagos Islands Fund Junior Research Fellowship at Christ's College, Cambridge. D.G.'s contribution is based upon work while serving at the National Science Foundation and was funded by NSF grant no. EAR-1145271.

Acknowledgements. We acknowledge the Royal Society of London who supported the Hooke meeting. Iris Buisman is thanked for the support in obtaining and manipulating the QEMSCAN data and images. We thank two anonymous referees for their thoughtful and insightful comments which greatly improved an earlier version of this contribution.

References

1. Marsh B. 2004 A magmatic mush column rosetta stone: the McMurdo Dry Valleys of Antarctica. *Eos Trans. Am. Geophys. Union* **85**, 497–502. (doi:10.1029/2004EO470001)
2. Christopher TE, Blundy J, Cashman K, Cole P, Edmonds M, Smith PJ, Sparks RSJ, Stinton A. 2015 Crustal-scale degassing due to magma system destabilization and magma-gas decoupling at Soufrière Hills Volcano, Montserrat. *Geochem. Geophys. Geosyst.* **16**, 2797–2811. (doi:10.1002/2015GC005791)
3. Cashman KV, Sparks RSJ, Blundy JD. 2017 Vertically extensive and unstable magmatic systems: a unified view of igneous processes. *Science* **355**, eaag3055. (doi:10.1126/science.aag3055)
4. McBirney AR, Noyes RM. 1979 Crystallization and layering of the Skaergaard intrusion. *J. Petrol.* **20**, 487–554. (doi:10.1093/petrology/20.3.487)
5. Bachmann O, Bergantz GW. 2004 On the origin of crystal-poor rhyolites: extracted from batholithic crystal mushes. *J. Petrol.* **45**, 1565–1582. (doi:10.1093/petrology/egh019)
6. Salmonsen LP, Tegner C. 2013 Crystallisation sequence of the Upper Border Series of the Skaergaard Intrusion: revised subdivision and implications for chamber-scale magma homogeneity. *Contrib. Mineral. Petrol.* **165**, 1155–1171. (doi:10.1007/s00410-013-0852-y)
7. Wager LR, Deer WA. 1939 Geological investigations in East Greenland. Part III. The petrology of the Skaergaard intrusion, Kangerdlussuaq, East Greenland. *Meddelelser om Grønland* **105**, 352.
8. Holness MB, Farr R, Neufeld JA. 2017 Crystal settling and convection in the Shiant Isles Main Sill. *Contrib. Mineral. Petrol.* **172**, 7. (doi:10.1007/s00410-016-1325-x)
9. Namur O, Humphreys MCS, Holness MB. 2014 Crystallisation of interstitial liquid and latent heat buffering on solidifying gabbros: Skaergaard Intrusion, Greenland. *J. Petrol.* **55**, 1389–1427. (doi:10.1093/petrology/egu028)
10. Holness MB, Richardson C, Andersen J. 2013 The campsite dykes: a window into the early post-solidification history of the Skaergaard intrusion, East Greenland. *Lithos* **182–183**, 134–149. (doi:10.1016/j.lithos.2013.10.007)
11. Holness MB, Namur O, Cawthorn RG. 2013 Disequilibrium dihedral angles in layered intrusions: a microstructural record of fractionation. *J. Petrol.* **54**, 2067–2093. (doi:10.1093/petrology/egt041)
12. Scoates JS, Lindsley DH, Frost BR. 2010 Magmatic and structural evolution of an anorthositic magma chamber: the Poe Mountain intrusion, Laramie Anorthosite Complex, Wyoming. *Can. Mineral.* **48**, 851–885. (doi:10.3749/canmin.48.4.851)
13. Irvine TN, Andersen JCØ, Brooks CK. 1998 Included blocks (and blocks within blocks) in the Skaergaard intrusion: geological relations and the origins of rhythmic

modally graded layers. *Bull. Geol. Soc. Am.* **110**, 1398–1447. (doi:10.1130/0016-7606(1998)110<1398:IBABWB>2.3.CO;2)
14. Vukmanovic Z, Holness MB, Monks K, Andersen JCØ. 2018 The Skaergaard trough layering: sedimentation in a convecting magma chamber. *Contrib. Mineral. Petrol.* **173**, 43. (doi:10.1007/s00410-018-1466-1)
15. Solgadi F, Sawyer EW. 2008 Formation of igneous layering in granodiorite by gravity flow: a field, microstructure and geochemical study of the Tuolumne Intrusive Suite at Sawmill Canyon, California. *J. Petrol.* **49**, 2009–2042. (doi:10.1093/petrology/egn056)
16. Grout FF. 1918 Internal structures of igneous rocks; their significance and origin; with special reference to the Duluth Gabbro. *J. Geol.* **26**, 439–458. (doi:10.1086/622605)
17. Higgins MD. 1991 The origin of laminated and massive anorthosite, Sept Iles layered intrusion, Quebec, Canada. *Contrib. Mineral. Petrol.* **106**, 340–354. (doi:10.1007/BF00324562)
18. Meurer W, Boudreau A. 1998 Compaction of igneous cumulates part II: compaction and the development of igneous foliations. *J. Geol.* **106**, 293–304. (doi:10.1086/516023)
19. O'Driscoll B, Hargraves R, Emeleus C, Troll V, Donaldson C, Reavy R. 2007 Magmatic lineations inferred from anisotropy of magnetic susceptibility fabrics in Units 8, 9, and 10 of the Rum Eastern Layered Series, NW Scotland. *Lithos* **98**, 27–44. (doi:10.1016/j.lithos.2007.01.009)
20. O'Driscoll B, Stevenson CT, Troll VR. 2008 Mineral lamination development in layered gabbros of the British Palaeogene Igneous Province: a combined anisotropy of magnetic susceptibility, quantitative textural and mineral chemistry study. *J. Petrol.* **49**, 1187–1221. (doi:10.1093/petrology/egn022)
21. VanTongeren JA, Hirth G, Kelemen PB. 2015 Constraints on the accretion of the gabbroic lower oceanic crust from plagioclase lattice preferred orientation in the Samail Ophiolite. *Earth Plan Sci. Lett.* **427**, 249–261. (doi:10.1016/j.epsl.2015.07.001)
22. Paterson SR, Fowler Jr TK, Schmidt KL, Yoshinobu AS, Yuan ES, Miller RB. 1998 Interpreting magmatic fabric patterns in plutons. *Lithos* **44**, 53–82. (doi:10.1016/S0024-4937(98)00022-X)
23. Wager LR. 1962 Igneous cumulates from the 1902 eruption of Soufriere, St. Vincent. *Bull. Volcanol.* **24**, 93–99. (doi:10.1007/BF02599333)
24. Becker HJ. 1977 Pyroxenites and hornblendites from the maar-type volcanoes of the Westeifel, Federal Republic of Germany. *Contrib. Mineral. Petrol.* **65**, 45–52. (doi:10.1007/BF00373569)
25. de Silva SL. 1989 The origin and significance of crystal rich inclusions in pumices from two Chilean ignimbrites. *Geol. Mag.* **126**, 159–175. (doi:10.1017/S0016756800006300)
26. Tait SR. 1988 Samples from the crystallising boundary layer of a zoned magma chamber. *Contrib. Mineral. Petrol.* **100**, 470–483. (doi:10.1007/BF00371376)
27. Tait SR, Wörner G, van den Bogaard P, Schminke HU. 1989 Cumulate nodules as evidence for convective fractionation in a phonolite magma chamber. *J. Volcan. Geotherm. Res.* **37**, 21–37. (doi:10.1016/0377-0273(89)90111-X)
28. Turbeville BN. 1993 Sidewall differentiation in an alkali magma chamber: evidence from syenite xenoliths in tuffs of the Latera caldera, Italy. *Geol. Mag.* **130**, 453–470. (doi:10.1017/S0016756800020537)
29. Holness MB, Bunbury JM. 2006 Insights into continental rift-related magma chambers: cognate nodules from the Kula Volcanic Province, Western Turkey. *J. Volcan. Geotherm. Res.* **153**, 241–261. (doi:10.1016/j.jvolgeores.2005.12.004)
30. Bachmann O. 2010 The petrologic evolution and pre-eruptive conditions of the rhyolitic Kos Plateau Tuff (Aegean arc). *C. Eur. J. Geosci.* **2**, 270–305.
31. Stock MJ, Taylor RN, Gernon TM. 2012 Triggering of major eruptions recorded by actively forming cumulates. *Sci. Rep.* **2**, 731. (doi:10.1038/srep00731)
32. Jakobsen JK, Tegner C, Brooks CK, Kent AJR, Lesher CE, Nielsen TFD, Wiedenbeck M. 2010 Parental magma of the Skaergaard intrusion: constraints from melt inclusions in primitive troctolitic blocks and FG-1 dykes. *Contrib. Mineral. Petrol.* **159**, 61–79. (doi:10.1007/s00410-009-0416-3)
33. Putirka KD. 2008 Thermometers and barometers for volcanic systems. *Rev. Mineral. Geochem.* **69**, 61–120. (doi:10.2138/rmg.2008.69.3)
34. Holness MB, Anderson AT, Martin VM, Maclennan J, Passmore E, Schwindinger K. 2007 Textures in partially solidified crystalline nodules: a window into the pore structure of slowly cooled mafic intrusions. *J. Petrol.* **48**, 1243–1264. (doi:10.1093/petrology/egm016)

35. Coombs ML, Eichelberger JC, Rutherford MJ. 2002 Experimental and textural constraints on mafic nodule formation in volcanic rocks. *J. Volcan. Geotherm. Res.* **119**, 125–144. (doi:10.1016/S0377-0273(02)00309-8)
36. Delaney PT, Pollard DD. 1982 Solidification of basaltic magma during flow in a dyke. *Am. J. Sci.* **282**, 856–885. (doi:10.2475/ajs.282.6.856)
37. Snyder D. 2000 Thermal effects of the intrusion of basaltic magma into a more silicic magma chamber and implications for eruption triggering. *Earth Plan Sci. Lett.* **175**, 257–273. (doi:10.1016/S0012-821X(99)00301-5)
38. Sisson TW, Bacon CR. 1999 Gas-driven filter pressing in magmas. *Geology* **27**, 613–616. (doi:10.1130/0091-7613(1999)027<0613:GDFPIM>2.3.CO;2)
39. Candela PA. 1991 Physics of aqueous phase evolution in plutonic environments. *Am. Min.* **76**, 1081–1091.
40. Bacon CR. 1986 Inclusions of mafic magma in intermediate and silicic volcanic rocks. *J. Geophys. Res.* **91**, 6091–6112. (doi:10.1029/JB091iB06p06091)
41. Thomas N, Tait SR. 1997 The dimensions of magmatic inclusions as a constraint on the physical mechanism of mixing. *J. Volcan. Geotherm. Res.* **75**, 167–178. (doi:10.1016/S0377-0273(96)00034-0)
42. Hartley ME, Morgan DJ, Maclennan J, Edmonds E, Thordarson T. 2016 Tracking timescales of short-term precursors to large basaltic fissure eruptions through Fe-Mg diffusion in olivine. *Earth Plan Sci Lett.* **439**, 58–70. (doi:10.1016/j.epsl.2016.01.018)
43. Lofgren G. 1974 An experimental study of plagioclase crystal morphology: isothermal crystallization. *Am. J. Sci.* **274**, 243–273. (doi:10.2475/ajs.274.3.243)
44. Holness MB. 2014 The effect of crystallization time on plagioclase grain shape in dolerites. *Contrib. Mineral. Petrol.* **168**, 1076. (doi:10.1007/s00410-014-1076-5)
45. Holness MB, Siklos STC. 2000 The rates and extent of textural equilibration in high-temperature fluid-bearing systems. *Chem. Geol.* **162**, 137–153. (doi:10.1016/S0009-2541(99)00124-2)
46. Hunter RH. 1987 Textural equilibrium in layered igneous rocks. In *Origins of igneous layering* (ed. I Parsons), pp. 473–503. D. Reidel Publishing Company.
47. Kruhl JH. 2001 Crystallographic control on the development of foam textures in quartz, plagioclase and analogue material. *Int. J. Earth Sci.* **90**, 104–117. (doi:10.1007/s005310000170)
48. Holness MB, Richardson C, Helz RT. 2012 Disequilibrium dihedral angles in dolerite sills: a new proxy for cooling rate. *Geology* **40**, 795–798. (doi:10.1130/G33119.1)
49. Holness MB. 2015 Plagioclase growth rates control three-grain junction geometry in dolerites and gabbros. *J. Petrol.* **56**, 2117–2144. (doi:10.1093/petrology/egv065)
50. Wager LR, Brown GM, Wadsworth WJ. 1960 Types of igneous cumulates. *J. Petrol.* **1**, 73–85. (doi:10.1093/petrology/1.1.73)
51. Irvine TN. 1980 Magmatic infiltration metasomatism, double diffusive fractional crystallisation and adcumulus growth in the Muskox Intrusion and other layered intrusions. In *Physics of magmatic processes* (ed. RB Hargraves), pp. 325–383. Princeton, NJ: Princeton University Press.
52. Sparks RSJ, Kerr RC, McKenzie DP, Tait SR. 1985 Postcumulus processes in layered intrusions. *Geol. Mag.* **122**, 555–568. (doi:10.1017/S0016756800035470)
53. Shirley DN. 1986 Compaction of igneous cumulates. *J. Geol.* **94**, 795–809. (doi:10.1086/629088)
54. Tharp TM, Loucks RR, Sack RO. 1998 Modeling compaction of olivine cumulates in the Muskox intrusion. *Am. J. Sci.* **298**, 758–790. (doi:10.2475/ajs.298.9.758)
55. Tegner C, Thy P, Holness MB, Jakobsen JK, Lesher CE. 2009 Differentiation and Compaction in the Skaergaard Intrusion. *J. Petrol.* **50**, 813–840. (doi:10.1093/petrology/egp020)
56. McKenzie D. 2011 Compaction and crystallization in magma chambers: towards a model of the Skaergaard Intrusion. *J. Petrol.* **52**, 905–930. (doi:10.1093/petrology/egr009)
57. Holness MB, Vukmanovic Z, Mariani E. 2017 Assessing the role of compaction in the formation of adcumulates: a microstructural perspective. *J. Petrol.* **58**, 643–674. (doi:10.1093/petrology/egx037)
58. Nicolas A. 1992 Kinematics in magmatic rocks with special reference to gabbros. *J. Petrol.* **33**, 891–915. (doi:10.1093/petrology/33.4.891)
59. Rutter EH. 1983 Pressure solution in nature, theory and experiment. *J. Geol. Soc.* **140**, 725–740. (doi:10.1144/gsjgs.140.5.0725)

60. McClay KR. 1977 Pressure solution and Coble creep in rocks and minerals: a review. *J. Geol. Soc.* **134**, 57–70. (doi:10.1144/gsjgs.134.1.0057)
61. Cooper MR, Hunter RH. 1995 Precision serial lapping, imaging and three-dimensional reconstruction of minus-cement and post-cementation intergranular pore-systems in the Penrith Sandstone of north-western England. *Min. Mag.* **59**, 213–220. (doi:10.1180/minmag.1995.059.395.06)
62. Hunter RH. 1996 Textural development in cumulate rocks. In *Layered intrusions* (ed. GA Cawthorn), pp. 77–101. Elsevier Science BV.
63. Marsh BD. 1988 Crystal size distribution (CSD) in rocks and the kinetics and dynamics of crystallization. I. Theory. *Contrib. Mineral. Petrol.* **99**, 277–291. (doi:10.1007/BF00375362)
64. Kirkpatrick RJ. 1975 Crystal growth from the melt: a review. *Am. Min.* **60**, 798–814.
65. Kirkpatrick RJ. 1981 Kinetics of crystallization of igneous rocks. *Rev. Mineral.* **8**, 321–398.
66. Beane R, Wiebe RA. 2012 Origin of quartz clusters in Vinalhaven granite and porphyry, coastal Maine. *Contrib. Mineral. Petrol.* **163**, 1069–1082. (doi:10.1007/s00410-011-0717-1)
67. Graeter KA, Beane RJ, Deering CD, Gravley D, Bachmann O. 2015 Formation of rhyolite at the Okataina Volcanic Complex, New Zealand: new insights from analysis of quartz clusters in plutonic lithics. *Am Min.* **100**, 1778–1789. (doi:10.2138/am-2015-5135)
68. Wassmann S, Stöckhert B. 2013 Rheology of the plate interface – dissolution precipitation creep in high pressure metamorphic rocks. *Tectonophysics* **608**, 1–29. (doi:10.1016/j.tecto.2013.09.030)
69. Means WD, Park Y. 1994 New experimental approach to understanding igneous texture. *Geology* **22**, 323–326. (doi:10.1130/0091-7613(1994)022<0323:NEATUI>2.3.CO;2)
70. Emeleus CH, Cheadle MJ, Hunter RH, Upton BGJ, Wadsworth WJ. 1996 The Rum layered suite. *Dev. Petrol.* **15**, 403–440. (doi:10.1016/S0167-2894(96)80014-5)
71. Nielsen TFD. 2004 The shape and volume of the Skaergaard intrusion, Greenland: implications for mass balance and bulk composition. *J. Petrol.* **45**, 507–530. (doi:10.1093/petrology/egg092)
72. Brothers R. 1964 Petrofabric analyses of Rhum and Skaergaard layered rocks. *J. Petrol.* **5**, 255–274. (doi:10.1093/petrology/5.2.255)
73. Gay P, Muir ID. 1962 Investigation of the feldspars of the Skaergaard intrusion, Eastern Greenland. *J. Geol.* **70**, 565–581. (doi:10.1086/626852)
74. Nwe YY. 1975 Aspects of the mineralogy of the Skaergaard intrusion, East Greenland. Unpublished PhD thesis, University of Cambridge.
75. Irvine T. 1983 Skaergaard trough-layering structures. *Yearb. Carnegie Inst. Wash.* **82**, 289–295.
76. Holness MB, Stripp G, Humphreys MCS, Veksler IV, Nielsen TFD, Tegner C. 2011 Silicate liquid immiscibility within the crystal mush: late-stage magmatic microstructures in the Skaergaard intrusion, East Greenland. *J. Petrol.* **52**, 175–222. (doi:10.1093/petrology/egq077)
77. Naslund HR. 1984 Petrology of the Upper Border Series of the Skaergaard Intrusion. *J. Petrol.* **25**, 185–212. (doi:10.1093/petrology/25.1.185)
78. McBirney AR. 1989 The Skaergaard layered series: I. Structure and average compositions. *J. Petrol.* **30**, 363–397. (doi:10.1093/petrology/30.2.363)
79. Hammer CU, Clausen HB, Frierich WL, Tauber H. 1987 The Minoan eruption of Santorini in Greece dated to 1645 BC? *Nature* **328**, 517. (doi:10.1038/328517a0)
80. Martin VM, Holness MB, Pyle DM. 2006 Textural analysis of magmatic enclaves from the Kameni Islands, Santorini, Greece. *J. Volcan. Geotherm. Res.* **154**, 89–102. (doi:10.1016/j.jvolgeores.2005.09.021)
81. Holness MB, Humphreys MCS, Sides R, Helz RT, Tegner C. 2012 Toward an understanding of disequilibrium dihedral angles in mafic rocks. *J. Geophys. Res.* **117**, B06207. (doi:10.1029/2011JB008902)
82. Bercovici H, Geist D, Harpp KS, Almeida M, Mahr J, Pimentel R, Cleary Z. 2016 A little island with a big secret: Isla Rábida, Galápagos. In *AGU fall meeting abstracts*, V53C-3117.
83. Swanson FJ, Baitis HW, Lexa J, Dymond J. 1974 Geology of Santiago, Rábida, and Pinzón Islands, *Galápagos. Bull. Geol. Soc. Am.* **85**, 1803–1810. (doi:10.1130/0016-7606(1974)85<1803:GOSRAP>2.0.CO;2)
84. Geist DJ, Fornari DJ, Kurz MD, Harpp KS, Adam Soule S, Perfit MR, Koleszar AM. 2006 Submarine Fernandina: magmatism at the leading edge of the Galápagos hot spot. *Geochem. Geophys. Geosyst.* **7**, Q12007. (doi:10.1029/2006GC001290)

85. Geist D, White WM, Albarede F, Harpp K, Reynolds R, Blichert-Toft J, Kurz MD. 2002 Volcanic evolution in the Galápagos: the dissected shield of Volcan Ecuador. *Geochem. Geophys. Geosyst.* **3**, 1061. (doi:10.1029/2002GC000355)[]
86. Geist DJ, Bergantz G, Chadwick WW. 2014 Galapagos magma chambers. In *The Galapagos: a natural laboratory for the earth sciences* (eds KS Harpp, E Mittelstaedt, N d'Ozouville, DW Graham), 204, 55 pp. Hoboken, NJ: John Wiley & Sons, Inc.
87. Davidge L, Ebinger C, Ruiz M, Tepp G, Amelung F, Geist D, Coté, D, Anzieta J. 2017 Seismicity patterns during a period of inflation at Sierra Negra volcano, Galápagos Ocean Island Chain. *Earth Plan Sci. Lett.* **462**, 169–179. (doi:10.1016/j.epsl.2016.12.021)
88. Glazner AF. 2014 Magmatic life at low Reynolds number. *Geology* **42**, 935–938. (doi:10.1130/G36078.1)
89. Clemens JD. 2015 Magmatic life at low Reynolds number. *Geology* **43**, e357. (doi:10.1130/G36512C.1)
90. Wiebe RA, Jellinek AM, Hodge KF. 2017 New insights into the origin of ladder dikes: implications for punctuated growth and crystal accumulation in the Cathedral Peak granodiorite. *Lithos* **277**, 241–258. (doi:10.1016/j.lithos.2016.09.015)